Nonequilibrium molecular dynamics approaches to transport properties and non-Newtonian fluid rheology

ARTICLE *in* INDUSTRIAL & ENGINEERING CHEMISTRY RESEARCH · MAY 1992

Impact Factor: 2.59 · DOI: 10.1021/ie00005a001

2 AUTHORS:

Peter T Cummings
Vanderbilt University
518 PUBLICATIONS **11,746** CITATIONS
SEE PROFILE

Denis J. Evans
Australian National University
310 PUBLICATIONS **14,753** CITATIONS
SEE PROFILE

REVIEWS

Nonequilibrium Molecular Dynamics Approaches to Transport Properties and Non-Newtonian Fluid Rheology

Peter T. Cummings*

Department of Chemical Engineering, Thornton Hall, University of Virginia, Charlottesville, Virginia 22903-2442

Denis J. Evans

Research School of Chemistry, Australian National University, P.O. Box 4, Canberra, A.C.T. 2601, Australia

In this paper, we review nonequilibrium and equilibrium molecular dynamics methods for computing transport coefficients (shear viscosity, thermal conductivity, and diffusivity) of fluids from a knowledge of pair interactions between molecules. We describe the application of the nonequilibrium methods to predicting transport properties in many systems of industrial interest and to the understanding of fundamental aspects of polymer rheology.

1. Introduction

Thermophysical properties play a key role in process design and optimization which in turn is one of the main technologies employed by the chemical industry in its efforts to reduce operating and development costs by shortening the time and reducing the uncertainty in going from process innovation at the bench scale to industrial-scale commercialization. Consequently, the development of accurate, widely applicable, predictive methods for thermophysical property estimation is an enduring goal of much of the thermophysical property research in chemical engineering.

No correlation for a given thermophysical property can be *both* accurate *and* widely applicable unless it is based on an understanding of the molecular processes determining that property. The recognition of this fact has led to several decades of chemical engineering thermodynamics research aimed at elucidating the microscopic basis for thermodynamic properties (Prausnitz et al., 1986; Gubbins et al., 1983) and applying the insight gained into the development of accurate, fundamentally based equations of state for fluid mixtures. Microscopic level simulation (in which the dynamics and/or configurational properties of a small, representative sample of fluid are simulated by computer to calculate macroscopic properties of interest and to study their origin in the interactions and structure of the fluid molecules) has played, and continues to play, a key role in understanding the relationship between microscopic interactions and macroscopic thermophysical properties.

With the increasing availability of computing power at decreasing cost, the past two decades have witnessed the emergence of molecular simulation techniques (Allen and Tildesley, 1987) as viable tools for understanding thermodynamic and transport properties at the molecular level. While there have been many reviews of the use of molecular simulation to compute thermodynamic properties, such as the monograph edited by Haile and Mansoori (Haile and Mansoori, 1983), relatively little attention has been paid to the now large body of research aimed at predicting transport properties using molecular simulation. In this paper, we review the application of nonequilibrium molecular dynamics (NEMD) (and, where appropriate, equilibrium molecular dynamics (EMD) algorithms) to the prediction and correlation of transport coefficients in Newtonian fluids. We will also review the application of NEMD methods to the understanding of rheological properties in non-Newtonian polymeric fluids. Our focus in this Review will be on applications of the NEMD algorithms which have hitherto not been the subject of a review. The recent monograph by Evans and Morriss (Evans and Morriss, 1990b) contains a thorough review of the algorithms themselves and the theoretical developments (such as linear and nonlinear response theory) that justify them but does not review applications of the algorithms to fluids other than the Lennard-Jones (LJ) and soft-sphere (SS) fluids. The LJ fluid consists of spherically symmetric molecules interacting via the intermolecular pair potential

$$u_{LJ}(r) = 4\epsilon\left[\left(\frac{\sigma}{r}\right)^{12} - \left(\frac{\sigma}{r}\right)^{6}\right] \quad (1)$$

where ϵ and σ are the depth and the zero of the potential, respectively, and r is the intermolecular separation while the spherically symmetric molecules in the SS fluid interact through the repulsive energy part only of an LJ potential

$$u_{SS}(r) = \epsilon\left(\frac{\sigma}{r}\right)^{12} \quad (2)$$

By contrast, in this paper we will review the application of NEMD algorithms to the calculation of transport properties in several systems of considerable technological importance: liquid metals, molecular liquids (composed of nonspherical molecules), supercritical fluids, and liquid water. As we shall see, when the effective intermolecular pair potentials are accurate enough, NEMD has proved to be an efficient and accurate tool for the prediction of

* Author to whom correspondence should be addressed.

0888-5885/92/2631-1237$03.00/0

transport properties such as shear viscosity, thermal conductivity, and diffusivity. In the next section, section 2, we briefly review both NEMD and EMD simulation algorithms. In section 3, we review applications of the algorithms to systems to technological interest. We conclude, in section 4, with a discussion of future research directions in NEMD simulation methodology.

This Review will be focused on the application of NEMD algorithms to the prediction of transport properties in bulk Newtonian and non-Newtonian systems. Thus, although EMD algorithms are briefly reviewed for completeness, no attempt will be made to comprehensively review applications of EMD algorithms. Rather, EMD applications will be discussed only in the context of systems for which NEMD methods have been applied. Furthermore, except for providing some historical perspective in the discussion of algorithm development, we will limit our review of NEMD algorithm applications of those algorithms which have proved to be most efficient and which have been validated by linear and nonlinear response theory.

2. Simulation Methodologies for Transport Phenomena

In this section, we briefly review molecular simulation methodologies for studying transport phenomena. The review is not meant to be comprehensive, but rather is designed to introduce the major concepts referred to in section 3.

Simulation methodologies for studying transport phenomena can be broadly categorized into equilibrium molecular dynamics (EMD) and nonequilibrium molecular dynamics (NEMD) techniques. The EMD techniques rely on computing equilibrium time correlation functions by measuring the decay of spontaneous fluctuations in properties of a fluid (the so-called Green–Kubo (GK) methods) or by measuring accumulated displacements in properties over time (essentially the integrated form of the GK relations, called Einstein relations). The NEMD technique involves measuring the response of a system to a perturbing field and relating the linear response to a transport coefficient. The GK relation for a given transport property involves calculating *equilibrium* autocorrelation functions for the relevant current. In NEMD we drive the system away from equilibrium and calculate the transport coefficient from the ratio of the current to the field. We now describe both EMD and NEMD techniques.

2.1. Equilibrium Molecular Dynamics Methods. A succint review of the formulas required for implementing EMD techniques to compute transport properties in fluids of spherically symmetric molecules is given by McQuarrie (McQuarrie, 1976). Here we summarize the main results. Extensions to molecular fluids (fluids composed of nonspherical molecules) and to mixtures are generally straightforward with the differences briefly noted where appropriate.

In order to use GK or Einstein relations, one performs an equilibrium molecular dynamics simulation using Newton's equations of motion or a variant thereof, such as the isokinetic equations of motion (Evans et al., 1983)

$$\frac{d\vec{r}_i}{dt} = \frac{\vec{p}_i}{m} \tag{3}$$

$$\frac{d\vec{p}_i}{dt} = \vec{F}_i - \alpha\vec{p}_i \tag{4}$$

In these equations, $\vec{r}_i$ is the position of the center of mass of molecule i, $\vec{p}_i$ is the linear momentum of molecule i, $\vec{F}_i$ is the force on the center of mass of molecule i (computed from the intermolecular potential), m is the mass of the molecule, t is time, and α, the thermostating multiplier, is given by

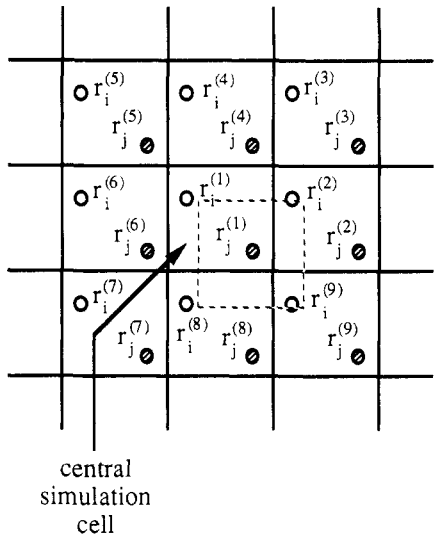

Figure 1. Periodic boundary conditions employed in molecular simulation. The central simulation cell (shown by arrow, molecular positions with superscript 1) is replicated infinitely in the x, y, and z directions. The minimum image convention means that molecular j interacts only with the images of molecules contained in the dashed box.

$$\alpha = \sum_{i=1}^{N} \vec{p}_i \cdot \vec{F}_i / \sum_{i=1}^{N} \vec{p}_i \cdot \vec{p}_i \tag{5}$$

The functional form of the thermostating term in eq 4 is derived using Gauss's principle of least constraint, and eq 5 ensures that the kinetic energy is a constant of the motion. [If $\alpha = 0$, we recover Newton's equations for which the total energy is a constant of the motion.] Other thermostating schemes (such as frequent momentum rescaling and the true conanical ensemble method of Nosé (Nosé, 1984a,b)) are used in practice. All three methods have been shown by Evans and Morriss (Evans and Morriss, 1984b; Morriss and Evans, 1985) to yield equivalent results in the linear response regime. Thus, equations of motion such as eqs 3–5 are used to generate equilibrium trajectories of a finite number N of molecules occupying volume V at temperature T. The equations of motion are supplemented by periodic boundary conditions to remove surface effects (Allen and Tildesley, 1987) as illustrated in Figure 1. For systems with short-range forces, molecule j interacts only with the images of molecules that fall inside a box centered at molecule j with the same dimensions as the central simulation cell. This is indicated by the dashed box shown in Figure 1. In the case of small, rigid nonspherical molecules, we supplement these translational equations of motion for the center of mass by the quaternionic rotational equations of motion for the angular degrees of freedom (Allen and Tildesley, 1987). These are given by

$$d\vec{L}_i/dt = \vec{T}_i$$

$$\vec{L}_i^{\,p} = \mathbf{A}_i\vec{L}_i$$

$$\omega_{i\beta}^{p} = L_{i\beta}^{p}/I_\beta, \quad \beta = x, y, z$$

$$\frac{d}{dt}\begin{pmatrix} q_{i1} \\ q_{i2} \\ q_{i3} \\ q_{i4} \end{pmatrix} = \frac{1}{2}\begin{pmatrix} -q_{i3} & -q_{i4} & q_{i2} & q_{i1} \\ q_{i4} & -q_{i3} & -q_{i1} & q_{i2} \\ q_{i1} & q_{i2} & q_{i4} & q_{i3} \\ -q_{i2} & q_{i1} & -q_{i3} & q_{i4} \end{pmatrix}\begin{pmatrix} \omega_{ix}^{p} \\ \omega_{iy}^{p} \\ \omega_{iz}^{p} \\ 0 \end{pmatrix} \tag{6}$$

In these equations, for molecule i, $\vec{\omega}_i$, $\vec{L}_i$, and $\vec{T}_i$ represent the angular velocity, angular momentum, and torque on the center of mass in the laboratory frame. The principal (or molecular) axis frame quantities have superscript p. The matrix $\mathbf{A}_i$ is the rotation matrix that converts the laboratory frame coordinates of molecule i to molecular frame coordinates and is a function of the orientation of the molecule. The $q_{i,j}$, $j = 1, ..., 4$ are the quaternions for representing the orientation of molecule i in such a way that the equations of motion are singularity-free (Evans, 1977). For mixtures, the mass m in eq 3 and the moments of inertia in eqs 6 would depend on molecule index i. For molecules with sufficient complexity—such as molecules with internal vibrational and/or rotational degrees of freedom and chain molecules (both rigid and flexible)—it is more appropriate (and computationally more efficient) to use algorithms such as SHAKE (Ryckaert et al., 1977; Ryckaert and Bellemans, 1978; Ciccotti et al., 1982) and the Gaussian constraint algorithm (Edberg et al., 1986, 1987; Morriss and Evans, 1991) in which the centers of force within a molecule (which may be the centers of atoms or functional groups) are treated as individual atoms and the intramolecular forces as algebraic constraints on their motion. Transport properties can then be calculated from these EMD trajectories using Einstein or GK relations.

Einstein relations can be derived by considering microscopic expressions for quantities (such as the mass density and momentum density), substituting these expressions into the corresponding macroscopic transport equation (such as Fick's law of diffusion or the Navier–Stokes equation incorporating Newton's law of viscosity) and solving for the transport coefficient of interest (such as diffusion coefficient and shear viscosity). The GK relations can be obtained either by manipulation of the corresponding Einstein relation or directly by using linear response theory (Zwanzig, 1965).

The Einstein relation for viscosity is given by

$$\eta = \lim_{t\to\infty} \frac{1}{2Vk_BTt} \left\langle \sum_{j=1}^{N} [z_j(t)\ p_{jx}(t) - z_j(0)\ p_{jx}(0)]^2 \right\rangle \quad (7)$$

where $\langle ... \rangle$ indicates equilibrium ensemble average, t is time, k_B is Boltzmann's constant, and $p_{l\alpha}$ and α_l ($l = 1, ..., N$, $\alpha = x, y, z$) are the α components of $\vec{p}_l$, and $\vec{r}_l$, respectively. As pointed out by Chialvo and Debenedetti (Chialvo and Debenedetti, 1991), there are several other forms of the Einstein formula for viscosity, with eq 7 being referred to by Chialvo and Debenedetti as the McQuarrie form. In particular, Chialvo and Debenedetti singled out what they denoted as the Helfand form

$$\eta = \lim_{t\to\infty} \frac{1}{2Vk_BTt} \left\langle \left[\sum_{j=1}^{N} z_j(t)\ p_{jx}(t) - z_j(0)\ p_{jx}(0)\right]^2 \right\rangle \quad (8)$$

[Strictly speaking, Chialvo and Debenedetti have

$$\lim_{t\to\infty} \frac{1}{t} \langle ... \rangle$$

replaced by the equivalent

$$\lim_{t\to\infty} \frac{d}{dt} \langle ... \rangle$$

in eqs 7 and 8.] The Helfand and McQuarrie expressions are equivalent in the thermodynamic limit of a system whose total linear momentum is zero. This equivalence hinges on a conjecture made by Chialvo and Debenedetti and recently proved by Chialvo et al. (Chialvo et al., 1992). Chialvo and Debenedetti believed that the McQuarrie form would be computationally more efficient since it sums N individual contributions at each time step while the Helfand expression involves only a single contribution at each time step, and indeed computationally the McQuarrie form has considerably less noise than the Helfand form (Chialvo and Debenedetti, 1991). However, Chialvo et al. (Chialvo et al., 1992) have shown that the viscosities predicted by both the Helfand and McQuarrie forms exhibit substantial size dependence so that the practical utility of either the Helfand or the McQuarrie form is now an open question. The GK relation for shear viscosity η is given by

$$\eta = \frac{V}{k_BT} \int_0^\infty \langle P_{xy}(0)\ P_{xy}(t) \rangle\ dt \quad (9)$$

where P_{xy} is the xy component of the pressure tensor $\mathbf{P}$ given by (Evans, 1979c, 1980, 1981a)

$$\mathbf{P}V = \frac{1}{m} \sum_{i=1}^{N} \vec{p}_i\vec{p}_i + \sum_{i=1}^{N} \vec{r}_i\vec{F}_i \quad (10)$$

The Einstein relation for the self-diffusion coefficient D_s is given by

$$D_s = \lim_{t\to\infty} \frac{\langle (\Delta r(t))^2 \rangle}{6t} \quad (11)$$

where $\langle (\Delta r(t))^2 \rangle$ is the equilibrium ensemble average of the quantity $(1/N)\sum_{i=1}^{N}[\vec{r}_i(t) - \vec{r}_i(0)]^2$ which is the mean squared displacement. The GK relation for D_s is

$$D_s = \frac{1}{3m^2} \int_0^\infty \langle \vec{p}(0)\cdot\vec{p}(t) \rangle\ dt \quad (12)$$

where $\langle \vec{p}(0)\cdot\vec{p}(t) \rangle$ is the equilibrium ensemble average of the quantity $(1/N)\sum_{i=1}^{N}\vec{p}_i(0)\cdot\vec{p}_i(t)$ which is the velocity (or momentum) autocorrelation function. The Einstein relation for the thermal conductivity λ is given by

$$\lambda = \lim_{t\to\infty} \frac{1}{6Vk_BT^2t} \left\langle \sum_{i=1}^{N} [\vec{r}_i(t)\ \tilde{E}_i(t) - \vec{r}_i(0)\ \tilde{E}_i(0)]^2 \right\rangle \quad (13)$$

where $\tilde{E}_i$ is the instantaneous excess energy of molecule i, $\tilde{E}_i = E_i - (1/N)\sum_{j=1}^{N}E_j$, where E_i is the total (kinetic plus potential) energy of molecule i. The corresponding GK relation is

$$\lambda = \frac{1}{3Vk_BT^2} \int_0^\infty \langle \vec{S}(t)\cdot\vec{S}(0) \rangle\ dt \quad (14)$$

where $\vec{S} = d/dt\sum_{i=1}^{N}\vec{r}_i\tilde{E}_i$.

2.2. Nonequilibrium Molecular Dynamics Methods. The general philosophy of the NEMD method (Evans and Morriss, 1990b) is to introduce a (usually fictitious) field X into the equations of motion of the system, which drives the conjugate thermodynamic flux J (such as the momentum flux in planar Couette flow or the heat current for thermal conductivity). The first requirement for this applied field is that it be consistent with periodic boundary conditions to ensure that the simulation sample remains homogeneous. The second requirement is that the transport property δ of interest can be calculated from the constitutive relation

$$\delta = \lim_{X\to 0} \lim_{t\to\infty} J/X \quad (15)$$

The formal proof that an algorithm satisfies these two requirements is given by linear response theory (Evans, 1986a). In many cases the value of the transport coefficient at nonzero fields has no physical meaning since the field used to drive the thermodynamic flux is fictitious. However, the sllod algorithm for planar Couette flow (Evans and Morriss, 1984b; Ladd, 1984) used to calculate shear

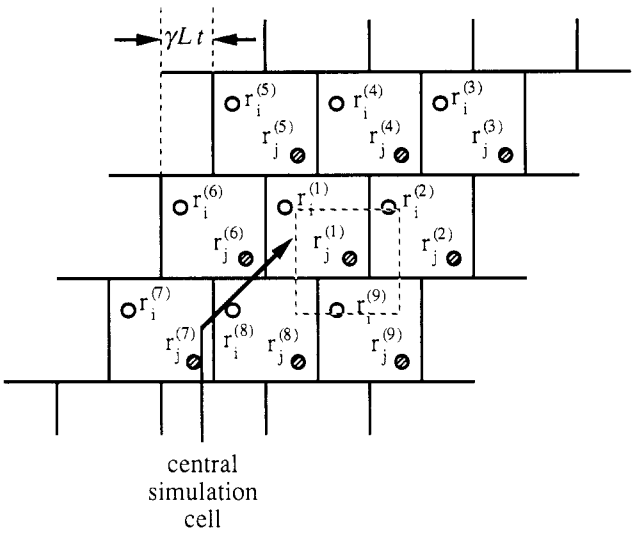

Figure 2. Sliding brick boundary conditions employed in NEMD simulations of planar Couette flow. The central simulation cell (shown by arrow, molecular positions with superscript 1) is replicated infinitely in the x, y, and z directions. The boxes above and below the central simulation cell move right and left (respectively) at velocities determined by the strain rate γ.

viscosity can be shown to be exact for all values of the field (which in this case is the velocity gradient represented by the strain rate $\gamma = \partial u_x/\partial y$, the rate of change of the streaming velocity in the x direction with vertical position). While NEMD methods have been in use for over two decades, two recent developments have been especially significant: first, algorithm development has been systematized to the point that knowledge of a GK relation leads directly to a corresponding NEMD algorithm (Evans, 1986a); second, the NEMD algorithms have now been put on a sound theoretical basis through linear and nonlinear response theory (Evans and Morriss, 1984b, 1990b; Morriss and Evans, 1985; Evans, 1982).

There have been many NEMD algorithms for viscosity (Ciccotti et al. 1976, 1979; Gosling et al., 1973; Singer et al., 1980) developed subsequent to the earliest, "natural" algorithm proposed by Ashurst and Hooever (Ashurst and Hoover, 1972; Hoover and Ashurst, 1975), which consisted of performing a simulation with Newton's equations of motion, momenta rescaled each time step (for thermostating purposes), and the planar Couette flow velocity profile imposed through relative movement of the upper and lower boundaries. However, the most efficient NEMD algorithms for shear viscosity are the two homogeneous algorithms developed in the past decade, the Dolls tensor method (Hoover et al., 1980) and the sllod algorithm (Ladd, 1984; Evans and Morriss, 1984a). These two algorithms are combined with Lees–Edwards sliding brick boundary conditions (Lees and Edwards, 1972) in which periodic images of the simulation cell above and below the central simulation cell are moved in opposite directions at velocities determined by the imposed velocity profile. These boundary conditions are illustrated in Figure 2. They give the same response in the linear regime and are therefore equivalent when applied to the computation of viscosity for Newtonian fluids. The sllod algorithm, however, has been shown to be exact for arbitrarily large strain rates (Evans and Morriss, 1984b, 1990b) and is thus appropriate for the study of the nonlinear, non-Newtonian regime. For this reason, we focus our attention on this algorithm. We quote the algorithm without derivation. The most complete description is found in the recent monograph by Evans and Morriss (Evans and Morriss, 1990b). The isokinetic sllod equations of motion are given by

$$\frac{d\vec{r}_i}{dt} = \frac{\vec{p}_i}{m} + \vec{r}_i \cdot \nabla \vec{u} \tag{16}$$

$$\frac{d\vec{p}_i}{dt} = \vec{F}_i - \vec{p}_i \cdot \nabla \vec{u} - \alpha \vec{p}_i \tag{17}$$

where $\vec{u} = (u_x,0,0)$ with $u_x = \gamma y$ is the velocity field corresponding to planar Couette flow and α, the thermostating constant, is given by

$$\alpha = \sum_{i=1}^{N} [\vec{p}_i \cdot \vec{F}_i - \gamma p_{ix} p_{iy}] / \sum_{i=1}^{N} \vec{p}_i \cdot \vec{p}_i \tag{18}$$

The momenta in eqs 16 and 17 are measured with respect to the streaming velocity of the fluid and are called peculiar momenta. These equations of motion are combined with the Lee–Edwards "sliding brick" boundary conditions (Lees and Edwards, 1972). Ignoring for the moment the isokinetic constraints (i.e., setting $\alpha = 0$), elimination of momentum between eqs 3 and 4 and between eqs 16 and 17 leads to the same Newtonian equation relating $\vec{r}_i$ and $\vec{F}_i$. Hence, use of the sllod algorithm can be regarded as equivalent to using the EMD equations, eqs 3 and 4, except at $t = 0$ (when the Couette velocity field is imposed) and for the use of the Lees–Edwards boundary conditions. Thus, the sllod algorithm truly generates boundary driven planar Couette flow, leading to the conclusion that it is correct to arbitrary order in the strain rate (Evans and Morriss, 1984b, 1990b). In order to obtain a good signal-to-noise ratio, with the NEMD algorithms it is necessary to use strain rates γ which are large enough to cause the shear viscosity to be strain rate dependent. In order to compute the shear viscosity of a Newtonian fluid using the sllod algorithm, after the simulation reaches steady state at a given strain rate γ, one computes and averages the pressure tensor, eq 10. The strain rate dependent shear viscosity is obtained from Newton's law of viscosity

$$\frac{\langle p_{yx} \rangle + \langle p_{xy} \rangle}{2} = -\eta \frac{\partial u_x}{\partial y} = -\eta\gamma \tag{19}$$

In this equation, $\langle ... \rangle$ indicates a time average of the enclosed quantity over the steady-state trajectories generated by the equations of motion. Operationally, the averages denoted by $\langle ... \rangle$ are computed by averaging over a single trajectory (or simulation) that has reached a steady state, while in principle one should average over an ensemble of such trajectories. The use of a single trajectory should suffice provided ergodicity (the equivalence of time and ensemble averages) is satisfied. At very high strain rates (well beyond the strain rates used in the studies described in this Review), in the so-called string phase of planar Couette flow (Evans and Morriss, 1990b), there is evidence to suggest that ergodicity breaks down. For the low to moderate strain rates employed in order to calculate Newtonian shear viscosity, evidence for the equivalence of steady-state time and ensemble averages is provided by the transient time correlation function approach to steady-state averages (Evans and Morriss, 1990a) whereby agreement between ensemble and time averages has been verified to 1 part in 10^3.

From kinetic and mode coupling theories, it is known that the strain rate dependence of the shear viscosity is linear in $\gamma^{1/2}$ (Kawasaki and Gunton, 1973; Yamada and Kawasaki, 1975; Ernst et al., 1978). Hence, to apply the sllod algorithm to a Newtonian fluid, one performs several simulations at differing strain rates γ and fits the resulting strain rate dependent viscosities to the equation

$$\eta = \eta_0 + \eta_1\gamma^{1/2} \tag{20}$$

The zero strain rate extrapolation of η, η_0, is thus the Newtonian viscosity. This procedure is illustrated in section 3 below.

The NEMD sllod algorithm for nonspherical molecules is very similar to eqs 16–18. One choice which must be made is whether to apply the strain field to the center of mass of the molecule (which we will refer to as the molecular sllod algorithm) or to the individual atoms in the molecule (which we will refer to as the atomic sllod algorithm). Either can be used; however, one must measure the pressure tensor in the simulation consistently with the method of applying the strain field. Ladd (Ladd, 1984) has noted that for molecular fluids there are two expressions one can write down for the pressure tensor: a molecular expression, which is the same as eq 10 when the momenta and positions are center of mass quantities for the molecules, and an atomic expression given by

$$\mathbf{P}^{\text{atom}}V = \sum_{i=1}^{N}\sum_{\beta=1}^{n}\frac{\vec{p}_i^{\beta}\vec{p}_i^{\beta}}{m_\beta} + \sum_{i=1}^{N}\sum_{\beta=1}^{n}\vec{r}_i^{\beta}\vec{F}_i^{\beta} \tag{21}$$

where n is the number of sites (centers of force) in a molecule, $\vec{r}_i^{\beta}$ is the position of site β in molecule i, $\vec{p}_i^{\beta}$ is the linear momentum of site β in molecule i, $\vec{F}_i^{\beta}$ is the force on site β in molecule i, and m_i is the mass associated with site β in molecule i. This is simply the pressure tensor computed assuming that the individual centers of force act as atoms. The difference between the values of the pressure tensor obtained from the molecular and atomic expressions is vanishingly small in the steady-state limit for systems which are not subject to external torques. Edberg et al. (Edberg et al., 1987) point out that if the strain field is applied to the centers of mass of the molecules, the appropriate formula to calculate the pressure tensor is the molecular expression, eq 10. If the strain field is applied to the atoms, then the appropriate expression for the pressure tensor is the atomic expression, eq 21. Along with Edberg et al., we shall choose to solve the molecular form of the sllod equations and to compute the pressure tensor from the molecular expression. In this case, if we are using the quaternionic equations of motion to describe the rotational motion of the molecules, then the molecular sllod equations are given by

$$\frac{d\vec{r}_i}{dt} = \frac{\vec{p}_i}{m} + \vec{r}_i\cdot\nabla\vec{u} \tag{22}$$

$$\frac{d\vec{p}_i}{dt} = \vec{F}_i - \vec{p}_i\cdot\nabla\vec{u} - \alpha\vec{p}_i \tag{23}$$

$$d\vec{L}_i/dt = \vec{T}_i$$

$$\vec{L}_i^{\text{p}} = \mathbf{A}_i\vec{L}_i$$

$$\omega_{i\beta}^{\text{p}} = L_{i\beta}^{p}/I_\beta,\ \beta = x, y, z$$

$$\frac{d}{dt}\begin{pmatrix} q_{i1}\\ q_{i2}\\ q_{i3}\\ q_{i4}\end{pmatrix} = \frac{1}{2}\begin{pmatrix} -q_{i3} & -q_{i4} & q_{i2} & q_{i1}\\ q_{i4} & -q_{i3} & -q_{i1} & q_{i2}\\ q_{i1} & q_{i2} & q_{i4} & q_{i3}\\ -q_{i2} & q_{i1} & -q_{i3} & q_{i4}\end{pmatrix}\begin{pmatrix}\omega_{ix}^{\text{p}}\\ \omega_{iy}^{\text{p}}\\ \omega_{iz}^{\text{p}}\\ 0\end{pmatrix} \tag{24}$$

For nonspherical molecules in which the rotational and internal degrees of freedom of the molecules make the quaternionic algorithm inefficient, one can combine the sllod equations for the center of mass motion straightforwardly with the Gaussian constraint algorithm (Edberg et al., 1987; Morriss and Evans, 1991). For mixtures of spherically symmetric molecules, one simply needs to take into account species type in the mass terms in the equations of motion. For mixtures of nonspherical molecules, the moment of inertia terms in the quaternionic equations of motion and the mass terms in the Gaussian constraint equations will carry species indices.

It is important to briefly note that the strain rate dependence given by eq 20 has not been confirmed experimentally for low molecular weight fluids such as argon and methane, since the strain rates required to obtain non-Newtonian (strain rate dependent) shear viscosity in such systems are $O(10^{10}$–$10^{12})$ s^{-1}, far beyond the strain rates achievable in the laboratory [$O(10^7)$ s^{-1} at most)]. Very recently, Dhont, van der Werff, and de Kruif (Dhont et al., 1989; van der Werff et al., 1989) measured the shear viscosity of sterically stabilized monodisperse silica spheres in a cyclohexane solvent. The osmotic pressure and low-density transport properties of the suspension are found to be in agreement with the corresponding results for the hard-sphere fluid at the same volume fraction as the silica spheres (de Kruif et al., 1985), so that the silica sphere dispersions are experimental realizations of a simple fluid system whose "molecules" are about 80 nm in diameter and have a "molecular mass" of 2×10^9 g mol^{-1} (based on a measured silica density of 1.74 g cm^{-3} (de Kruif et al., 1985)). For molecules of this size and mass, laboratory shear rates are predicted by NEMD to cause strain rate dependency in the shear viscosity. Van der Werff et al. (van der Werff et al., 1989) measured this strain rate dependent shear viscosity and confirmed the square root behavior given by eq 20.

Additional evidence for the validity of the strain rate dependent results obtained in NEMD simulations can be found in applications to long-chain alkane molecules. From a series of NEMD simulations of n-hexadecane, Berker et al. (Berker et al., 1991) estimated the critical strain rate of n-hexadecane, the lowest strain rate at which power law (shear thinning) behavior begins. They compared this to the predicted critical strain rate from Rouse dynamics developed for polymeric melts and which has been validated by experiment. The NEMD and Rouse theory predictions were consistent, suggesting that NEMD predicts correctly the onset of non-Newtonian behavior.

The NEMD algorithm for self-diffusion is known as the color conductivity algorithm (Evans et al., 1983). The molecules are subjected to a fictitious color field F in the x direction by adding an external field term to the many-body Hamiltonian H_0

$$H = H_0 - \sum_{i=1}^{N} q_i x_i F \tag{25}$$

In this equation, q_i is the color "charge" on molecule i, $q_i = (-1)^i$. From Hamilton's equations, the translational equations of motion are given by

$$d\vec{r}_i/dt = \vec{p}_i/m \tag{26}$$

$$dp_{xi}/dt = F_{xi} - Fq_i$$

$$dp_{yi}/dt = F_{yi} - \lambda_s p_{yi}$$

$$dp_{zi}/dt = F_{zi} - \lambda_s p_{zi} \tag{27}$$

The time-varying external color field F drives the color current J_x and its instantaneous value is determined by the constraint that the color current J_x

$$J_x = \sum_i c_i\frac{p_{ix}}{m} \tag{28}$$

be time invariant. The thermostating constraint parameter, λ_s, is obtained by requiring that the kinetic energy

due to motion in the y and z directions is fixed. These two considerations lead to

$$F = \frac{1}{N}\sum_i c_i F_{xi}$$

$$\lambda_s = \sum_i (p_{iy}F_{iy} + p_{iz}F_{iz}) / \sum_i (p_{iy}^2 + p_{iz}^2) \quad (29)$$

The work P_d generated by the field F is given by

$$P_d = F\sum_i c_i p_{xi} \quad (30)$$

The self-diffusion coefficient, D_s, is then obtained from

$$D_s = -\frac{(N-1)}{N^2}\frac{J_c^2}{\langle P_d \rangle} k_B T \quad (31)$$

The color conductivity algorithm for nonspherical molecules is obtained by using the set of equations given above for the center of mass motion and the usual equilibrium equations of motion for the intramolecular and/or rotational degrees of freedom. An alternate form of the color field algorithm which features a thermostating multiplier on each coordinate direction is given in section 6.2 of Evans and Morriss (1990b).

The NEMD algorithm for computing the thermal conductivity of simple fluids was developed by Evans (Evans, 1982; Evans, 1986b) and involves the use of a fictitious vector field $\vec{F}$ as the driving force for a heat flux $\vec{J}_Q$. The equations of motion for an atomic system are

$$\frac{d\vec{r}_i}{dt} = \frac{\vec{p}_i}{m} \quad (32)$$

$$\frac{d\vec{p}_i}{dt} = \vec{F}_i + (E_i - E)\vec{F}(t) - \sum_{j=1}^{N} \vec{F}_{ij}\vec{r}_{ij}\cdot\vec{F}(t) + \frac{1}{2N}\sum_{j=1}^{N}\sum_{k=1}^{N} \vec{F}_{jk}\vec{r}_{jk}\cdot\vec{F}(t) - \alpha\vec{p}_i \quad (33)$$

where $\vec{F}_{ij}$ is the force exerted by molecule j on molecule i, E_i is the instantaneous energy of molecule i, $E = (1/N)\sum_{i=1}^{N} E_i$, $\vec{r}_{ij} = \vec{r}_j - \vec{r}_i$, and α is the thermostating multiplier given by

$$\alpha = \sum_i \left[\vec{F}_i + (E_i - E)\vec{F} - \frac{1}{2}\sum_j \vec{F}_{ij}\vec{r}_{ij}\cdot\vec{F} + \frac{1}{2N}\sum_{j,k} \vec{F}_{jk}\vec{r}_{jk}\cdot\vec{F} \right]\cdot\vec{p}_i \Big/ \sum_i \vec{p}_i\cdot\vec{p}_i \quad (34)$$

The heat current $\vec{J}_Q$ is then given by

$$\vec{J}_Q V = \frac{1}{m}\sum_i E_i\vec{p}_i - \frac{1}{2m}\sum_{ij}\vec{r}_{ij}\vec{p}_i\cdot\vec{F}_{ij} \quad (35)$$

and the thermal conductivity λ by the constitutive relation

$$\vec{F}\lambda = \vec{J}_Q / T \quad (36)$$

Using this method, Evans was able to determine the thermal conductivity of argon (modeled as a LJ fluid) at the triple point to higher precision than has been achieved experimentally. Consequently, when accurate effective pair potentials are available this method shows particular promise. A similar NEMD algorithm has been derived by Gillan and Dixon (Gillan and Dixon, 1983) from a quite different viewpoint.

For nonspherical molecules, the algorithm for thermal conductivity has been given by Evans and Murad (Evans and Murad, 1989). The equations of motion are the same as those for simple fluids, eqs 32 and 33, supplemented with equations of motion for rotational and intramolecular degrees of freedom. The main difference is in the expression for the heat flux, which for nonspherical molecules is given by

$$\vec{J}_Q V = \frac{1}{m}\sum_i E_i\vec{p}_i - \frac{1}{2m}\sum_{ij}\vec{r}_{ij}(\vec{p}_i\cdot\vec{F}_{ij} + \vec{\omega}_i^{\,p}\cdot\vec{T}_{ij}^{\,p}) \quad (37)$$

In this equation, $\vec{\omega}_i^{\,p}$ is the angular velocity of molecule i in the principal axis frame and $\vec{T}_{ij}^{\,p}$ is the torque exerted by molecule j on molecule i in the principle axis frame of molecule i.

The extension of the NEMD algorithms for diffusion and thermal conductivity to mixtures is not straightforward. The complication in developing NEMD methods for mixtures is the necessity to remove mass flux contributions from heat currents and heat flux contributions from any diffusive currents induced by external fields. Thus, one needs to consider heat and matter transport simultaneously in a NEMD context, which has the advantage of incidently yielding the cross coefficients (Soret and Dufour). MacGowan and Evans (MacGowan and Evans, 1986) derived a NEMD algorithm for thermal diffusion which permitted the calculation of the self and mutual diffusion coefficients in a LJ mixture (MacGowan and Evans, 1986; MacGowan, 1986) modeling equimolar argon–krypton in a dense liquid state. The results for the self and mutual diffusion coefficients were about 15% below the EMD GK results of Schoen and Hoheisel (Schoen and Hoheisel, 1984a,b). The discrepancy between the EMD and NEMD results has yet to be resolved and requires further study. Evans and MacGowan (Evans and MacGowan, 1987) subsequently pointed out an inconsistency in the microscopic definition of the energy current density used in the algorithm which affects the Soret and Dufour cross coefficients. Evans and Cummings (Evans and Cummings, 1990) recently introduced a modified thermal diffusion algorithm which corrects this problem. The algorithms are notationally complex, and we refer the interested reader to the original papers (MacGowan and Evans, 1986; Evans and MacGowan, 1987; Evans and Cummings, 1990) for the precise formulation of these algorithms. Recently, Sarman and Evans (Sarman and Evans, 1991) implemented the Evans/Cummings thermal diffusion algorithm to Ar–Kr mixtures. Because this is a highly ideal mixture, the obtained results are similar to those from the MacGowan/Evans algorithm. They also found consistency between the NEMD and GK results for this system, though the noise in the GK results for the cross coefficients was considerably higher than in the NEMD results.

This completes our survey of EMD and NEMD algorithms for calculating transport properties. In the next section, we will consider applications of these algorithms to several classes of fluids. Before doing so, however, we point out that the GK relations and the NEMD algorithms above are both special cases (zero external field in the case of the GK relations, long-time steady-state limit in the NEMD case) of more general relations which are derived using nonlinear response theory. The equations of motion used in NEMD of simple fluids are all of the form

$$\frac{d\vec{r}_i}{dt} = \frac{\vec{p}_i}{m} + C_i\vec{F}_e \quad (38)$$

$$\frac{d\vec{p}_i}{dt} = \vec{F}_i + D_i\vec{F}_e - \alpha\vec{p}_i \quad (39)$$

where $\vec{F}_e$ is the external field driving the system away from equilibrium and α is the usual thermostating multiplier. We are interested in calculating transport coefficients $L = L(F_e)$ defined in constitutive relations of the form

$$\vec{J} = -L(F_e)\vec{F}_e \tag{40}$$

The GK relations, given above, give relations between the limiting zero field transport coefficient, $L(F_e=0)$, and time integrals of fluctuations in the dissipative flux evaluated with the external field turned off. The GK expressions are special cases of more general relations for $L(F_e)$ valid at finite field known as transient time correlation functions (TTCFs). The TTCF relates the nonlinear, finite field transport coefficient to fluctuations in the dissipative flux evaluated during transients leading to the establishment of the steady state from the initial state. It is given by

$$L(F_e) = -\frac{1}{k_B T V}\int_0^\infty \langle \vec{J}(0)\cdot\vec{J}(s)\rangle_{F_e}\, ds \tag{41}$$

where $\langle ... \rangle_{F_e}$ denotes that the average is to be performed with the field turned on.

Because the TTCFs are evaluated with the applied field on, they require an NEMD simulation to be carried out. However, clearly in the limit of zero field they reduce to the GK relations for linear response. When TTCF calculations are performed at zero field, they are identical to GK calculations. The TTCF relations not only generalize the GK expressions to the nonlinear regime but they act as a bridge between EMD and NEMD. Because their derivation is relatively new, they have not been applied to systems other than the LJ and SS fluids. However, they are the most efficient means of studying small field nonlinearities since standard NEMD becomes inefficient at small field. [For example, the shear stress at very low strain rate has been studied using the differential version of the TTCF technique (Evans and Morriss, 1987) in which TTCFs in the presence and absence of a strain field are subtracted to determine the nonlinear response.] The TTCF approach should also prove useful for studying time-dependent phenomena such as stress overshoot (see section 3.2 below).

3. Applications of NEMD

In this section, we review the application of NEMD algorithms (and, where appropriate, EMD algoithms) to the computation of transport coefficients in Newtonian fluids and to the study of non-Newtonian fluid rheology.

3.1. Transport Properties of Newtonian Fluids from NEMD. Our interest is in the prediction of the transport properties of Newtonian (low molecular weight) fluids using NEMD. First, however, we will compare the performance of NEMD algorithms with EMD techniques.

3.1.1. Comparison of NEMD and EMD Methods. For shear viscosity, the only published direct comparison between NEMD and EMD is the study by Holian and Evans (Holian and Evans, 1983) comparing an NEMD algorithm (which predates the sllod algorithm) with the GK technique. The system studied was a LJ fluid at a high-temperature, high-density state some distance from the melting line. The GK results were found to exhibit substantial, nonmonotonic system size dependence, while the NEMD results showed little size dependence above 100 molecules. Moreover, the GK results were found to agree with the NEMD results only when large systems (approximately 4000 molecules) were used. This suggests that for shear viscosity NEMD is considerably more efficient than the EMD GK method. More recently, Hoheisel (Hoheisel, 1985) compared the shear viscosity of the LJ fluid computed using the EMD GK formula with NEMD results and found good agreement over a wide range of state points. The EMD GK results were found to be relatively insensitive to system size beyond approximately 500 molecules. The Einstein formula for shear viscosity, eq 7, has rarely been used in practice. One exception is its use by Alder et al. (Alder et al., 1970) in calculating the shear viscosity of hard spheres, where it has an advantage over the GK formula because it does not explicitly require the handling of collisions. Two other exceptions are the recent work by Debenedetti and co-workers (Chialvo et al., 1989) on the thermodynamic and transport properties of linear molecules and by Chialvo and Debenedetti (Chialvo and Debenedetti, 1991) on the LJ fluid. The Einstein formula appears to give low-noise predictions for the shear viscosity; however, for linear molecules there is some disagreement with corresponding NEMD simulations performed in our research group (Wang and Cummings, 1989a) and the Chialvo–Debenedetti results for the LJ fluid are in disagreement with NEMD and GK calculations. Chialvo et al. (Chialvo et al., 1992) have demonstrated and theoretically analyzed a strong system size dependence in the Einstein formula results for the LJ fluid. The computational practicality of the Einstein expressions is therefore an important open question currently under investigation in our laboratory. Thus, while the Holian–Evans study seems to favor NEMD over GK, it is not yet clear whether or not the Einstein method represents a significant improvement over GK.

For self-diffusion, the Einstein formula is an easily implemented and apparently reliable method for computing D_s and is the most frequently used. Unpublished results from our laboratory find that the EMD (Einstein and GK) and NEMD methods yield very consistent results for self-diffusion in the LJ fluid and in supercritical carbon dioxide (nonspherical molecules). To obtain the same degree of accuracy in D_s, the Einstein and GK techniques typically require fewer time steps than the color field NEMD algorithm, since the latter involves computing the color-field-dependent diffusion coefficient at several values of the color field and extrapolating to zero color field. Evans et al. (Evans et al., 1983) compared two NEMD algorithms for D_s with the GK algorithm for the LJ fluid at a state point near the triple point, finding that the NEMD value was a little below the GK result. Erpenbeck (Erpenbeck, 1987) found that, in order to obtain better than 2% agreement between GK and NEMD for the LJ fluid at the triple point, both simulations needed to be performed on large systems (>1000 molecules).

Thermal conductivity is perhaps the least studied of the three major transport properties. Alder et al. (Alder et al., 1970) computed the thermal conductivity of the hard sphere fluid using the Einstein formula, eq 13. Levesque and Verlet (Levesque and Verlet, 1987) describe extensive EMD GK simulations of η and λ at the LJ triple point including size dependence in systems containing up to 4000 molecules. They conclude that in the vicinity of the melting line large numbers of molecules are required by the GK method. Evans (Evans, 1986b) computed the thermal conductivity of the LJ fluid at the triple point, at the critical point, along the melting line, and at supercritical dense states. The results were compared to experimental data on argon and found to agree except near the critical point. Evans considered only 108 and 256 molecules, but found little difference between the two system sizes. However, in the absence of a direct comparison between Einstein, GK, and NEMD, there is no clear preference between the three methods, although the Levesque and Verlet results suggest that GK may not be efficient at high densities (since it requires large numbers of molecules in the simulation cell).

The basic tradeoff between EMD and NEMD techniques reduces to two considerations. First, theory shows

Table I. Summary of Transport Properties Obtained for Various Fluids in our Research Group by NEMD Compared with Experimental Data

fluid	potential	T, K	ρ, g cm^{-3}	property	NEMD	expt	error, %
CH_4	Williams	285.7	0.288	η	0.0376 cP	0.0377 cP	−0.3
	LJ	285.7	0.288		0.0421 cP	0.0377 cP	11.7
CH_4	Williams	100.0	0.439	η	0.105 cP	0.156 cP	−32.7
		130.0	0.394		0.068 cP	0.081 cP	−16.0
		160.0	0.336		0.045 cP	0.046 cP	−2.2
Rb	Price	318.9	1.501	η	0.690 cP	0.644 cP	7.1
		625.5	1.323		0.215 cP	0.234 cP	−8.1
		939.9	1.181		0.138 cP	0.155 cP	−11.0
Na	Swanson	500.0	1.006	η	0.48 cP	0.50 cP	4.0
		1000.0	1.006		0.23 cP	0.25 cP	8.0
		500.0	0.654		0.41 cP	0.45 cP	−8.9
		500.0	0.920		0.35 cP	0.43 cP	−18.6
		1000.0	0.920		0.25 cP	0.22 cP	13.6
H_2O	SPC	303.2	0.9957	η	0.428 cP	0.798 cP	−46.4
			1.0340		0.461 cP	0.801 cP	−42.4
			1.0681		0.491 cP	0.805 cP	−39.0
			1.1216		0.539 cP	0.831 cP	−35.1
CO_2	LJ	313.0	0.200	η	0.024 cP	0.021 cP	14.3
			0.841		0.107 cP	0.079 cP	35.4
			0.992		0.249 cP	0.118 cP	111
CO_2	2-site	313.0	0.200	η	0.024 cP	0.021 cP	14.3
			0.841		0.070 cP	0.079 cP	−11.4
			0.992		0.100 cP	0.118 cP	−15.3
CO_2	3-site	313.0	0.200	η	0.025 cP	0.021 cP	19.0
			0.841		0.077 cP	0.079 cP	−2.5
			0.992		0.132 cP	0.118 cP	11.9
CO_2	1-site	313.0	0.841	λ	53 W/(mK)	98 W/(mK)	−45.9
			0.992		80 W/(mK)	126 W/(mK)	−36.5
CO_2	3-site	313.0	0.841	λ	82 W/(mK)	98 W/(mK)	−16.3
			0.992		123 W/(mK)	126 W/(mK)	−2.4
CO_2	1-site	313.0	0.200	D_s	11.5 cm^2/s	10 cm^2/s	15.0
			0.841		1.83 cm^2/s	1.0 cm^2/s	83.0
			0.992		1.15 cm^2/s	unavailable	
CO_2	3-site	313.0	0.200	D_s	9.4 cm^2/s	10 cm^2/s	−6.0
			0.841		1.4 cm^2/s	1.0 cm^2/s	40.0
			0.992		0.92 cm^2/s	unavailable	

that the stress, velocity, and particle energy autocorrelation functions in the GK relations decay with long-time tails ($\sim t^{-3/2}$ as $t \to \infty$), so that the integrations in eqs 9, 12, and 14 when truncated at finite $t = \tau$ contain truncation errors of order $\tau^{-1/2}$. The long time tail problem becomes increasingly severe as the melting line is approached. Second, the autocorrelation functions (such as $\langle \vec{v}(t) \cdot \vec{v}(0) \rangle$) decay to zero at large t, thus becoming less accurate with increasing t because of errors introduced by the numerical integration scheme. These two effects appear to be the source of the requirement for reasonably long simulation runs of large numbers of molecules in EMD calculations. For NEMD, it appears that one can obtain accurate results for a given applied external field strength with considerably fewer molecules. However, with NEMD one must perform the simulation at several field strengths in order to extrapolate to zero field, reducing somewhat the advantage of the smaller system size. Additionally, it should be pointed out that all the transport coefficients can be calculated from a single EMD simulation (using Einstein and/or GK methods) whereas with NEMD a set of simulations must be performed for each transport property.

Thus, while it is not clear that NEMD is superior to EMD in efficiency in computing Newtonian transport coefficients, for smaller system sizes NEMD appears to be more accurate. In addition, the NEMD sllod equations permit the study of nonlinear (i.e., non-Newtonian) rheology while the EMD techniques do not. For these reasons, we have adopted the NEMD methods in our laboratory as the primary means for computing transport properties.

The application of NEMD to predicting transport properties in Newtonian fluids has been quite limited to date, since much of the work in this area has focussed on algorithm development rather than on applications. The recent monograph of Evans and Morriss provides an excellent review of these efforts (Evans and Morriss, 1990b). In developing and testing algorithms, researchers have usually performed simulations of the LJ or SS fluid. Thus, there exists a considerable body of results for the shear viscosity, thermal conductivity, and self-diffusion coefficient of the LJ and SS fluids (Evans et al., 1983; Holian and Evans, 1983; Evans, 1986b; Evans and Hanley, 1980; Evans and Watts, 1980). Comparison of the LJ results with experimental data on argon usually leads to good agreement except near the critical point (Evans, 1986b). Heyes (Heyes, 1987, 1988) also reports a table of LJ and SS transport properties obtained by both NEMD and EMD methods.

Many of the applications of NEMD to the prediction of transport properties for fluids of engineering interest have been performed in our laboratory at the University of Virginia. The main results from our laboratory (some of which are previously unpublished) are summarized in Table I.

3.1.2. Supercritical and Liquid Methane. The first calculation performed by Simmons and Cummings (Simmons and Cummings, 1986) was of the shear viscosity of supercritical dense methane (temperature 285.7 K and density 0.288 g cm^{-3}) using the methane intermolecular potential designed by Williams (Williams, 1967) to reproduce the liquid-state thermodynamic properties and the solid-state lattice energies of methane. [Evans (Evans, 1979b) also studied this same model at the same state conditions using an earlier version of the NEMD algorithms with much the same results as those reported by Simmons and Cummings.] In Figure 3, the straight line is the least-squares fit of the NEMD simulation results to

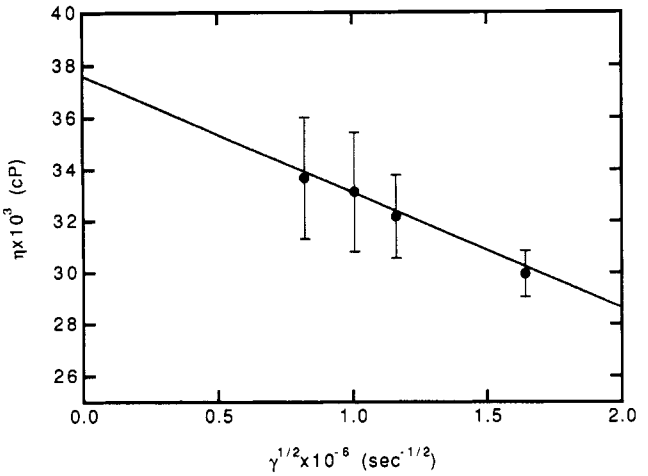

Figure 3. Shear viscosity η of methane at 285.7 K and 0.288 g cm^{-3} as a function of the square root of the strain rate γ. The circles and the error bars represent the simulation results and their estimated standard deviation, respectively.

Table II. NEMD Results for the Williams Potential Model of CH_4 along the Saturated Liquid Line Isotherm

ρ, g cm^{-3}	T, K	γ^*	time steps	p, atm	$u^{conf}/(Nk_BT)$	η, cP
0.439	100	4.0	20000	952.2	-7.807	0.0549
		1.44	20000	218.8	-8.326	0.0724
		1.0	20000	93.8	-8.389	0.0782
		0.64	20000	12.1	-8.440	0.0856
		0.36	20000	-58.8	-8.482	0.0912
0.394	130	4.0	20000	694.0	-6.855	0.0448
		1.44	20000	157.8	-7.251	0.0547
		1.0	20000	86.0	-7.298	0.0557
		0.64	20000	17.8	-7.341	0.0615
		0.36	20000	3.3	-7.369	0.0593
0.336	160	4.0	20000	466.8	-5.698	0.0329
		1.44	20000	137.9	-5.997	0.0389
		1.0	20000	66.4	-6.041	0.0390
		0.64	20000	46.2	-6.070	0.0393
		0.36	20000	19.3	-6.070	0.0422

eq 20. The zero strain rate extrapolation of the simulation results yields the Newtonian viscosity of 3.76×10^{-4} P, which is within 1/3% of the experimental value. The Williams potential is a site–site potential which models the methane–methane interaction as the sum of one carbon–carbon, eight carbon–hydrogen, and sixteen hydrogen–hydrogen interactions, thus modeling the nonspherical shape of the methane molecule. Simmons and Cummings also performed NEMD simulations on a LJ model for methane (with $\epsilon/k_B = 217$ K and $\sigma = 3.559$ Å) (Maitland et al., 1981) and found that this model differed from the experimental results by 12%. These results suggested that the Williams potential (Williams, 1967) might be very accurate for predicting the transport properties of methane.

To test this idea, Cummings (unpublished, reported here for the first time) performed NEMD simulations of methane along the saturated liquid line using both the Williams potential and the LJ potential. The NEMD results for the Williams and LJ potentials along the saturated liquid line are given in Tables II and III, respectively. Note that in these tables, the strain rate is given in the dimensionless form

$$\gamma^* = \gamma(m\sigma^2/\epsilon)^{1/2}$$

where we have used the LJ parameters for ϵ and σ. The strain rate dependent viscosities for the Williams potential are shown in Figure 4. The zero strain rate extrapolations of the strain rate dependent viscosities, which are thus the

Table III. NEMD Results for the Lennard-Jones Simple Fluid Model of CH_4 (with $\epsilon/k_B = 217$ K and $\sigma = 3.559$ Å) along the Saturated Liquid Line

ρ, g cm^{-3}	T, K	γ^*	time steps	p, atm	$u^{conf}/(Nk_BT)$	η, cP
0.439	100	1.44	50000	-523.6	-10.639	0.0796
		1.0	50000	-726.1	-10.821	0.0883
		0.64	50000	-862.8	-10.974	0.0979
		0.36	50000	-957.3	-11.085	0.1071
0.394	130	1.44	50000	-451.5	-7.267	0.0608
		1.0	50000	-551.5	-7.428	0.0648
		0.64	50000	-605.3	-7.495	0.0667
		0.36	50000	-628.9	-7.527	0.0695
0.336	160	1.44	150000	-26.2	-7.960	1.47×10^{-6}
		1.0	200000	-106.3	-7.049	3.57×10^{-4}
		0.64	100000	-329.7	-5.307	0.0386
		0.36	100000	-330.8	-5.246	0.0455

Table IV. NEMD Simulation Results and Experimental Data for the Shear Viscosity of Methane along the Saturated Liquid Line[a]

T, K	ρ, g cm^{-3}	η,[b] cP	η,[c] cP	η_{expt}, cP
100	0.439	0.105	0.135	0.156
130	0.394	0.068	0.078	0.081
160	0.336	0.045		0.046

[a] The theoretical results are obtained using the Williams (Williams, 1967) and LJ potentials. [b] Williams potential. [c] Lennard-Jones potential.

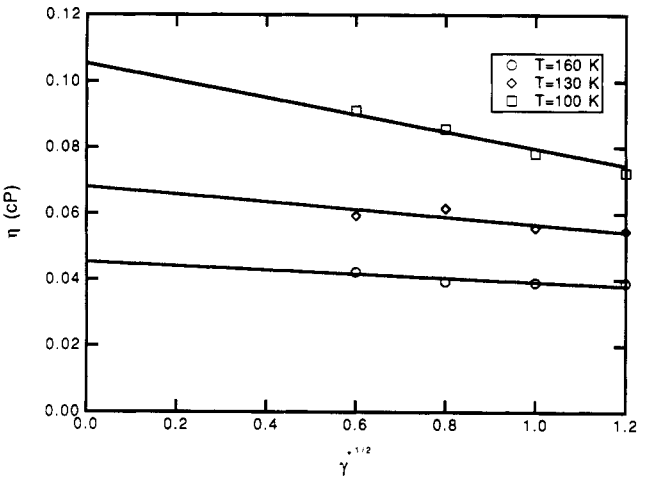

Figure 4. Shear viscosity η of methane along the saturated liquid line as a function of the square root of the reduced strain rate γ.

predictions for the Newtonian viscosity, for the LJ and Williams potential are given in Table IV. For the Williams potential, the predictions vary in accuracy from being within 2% of experiment at 160 K to 33% too low at 100 K. It thus appears that the Williams potential deteriorates in accuracy for predicting shear viscosity in the dense, low-temperature liquid regime. For the LJ potential, the predictions at 100 and 130 K are slightly better than for the Williams potential. At 160 K, the high strain rate viscosities predicted by the LJ fluid are anomalously low and no zero strain rate extrapolation can be reliably performed on the basis of the NEMD values. In fact, it is evident from the strongly negative pressures in Table III that the LJ fluid is well inside its two-phase region at each of the three states studied. For this reason, we do not regard the LJ fluid as a good model for methane along the saturated liquid line.

3.1.3. Liquid Metals. In a pair of papers, Cummings and Morriss (Cummings and Morriss, 1987, 1988) studied the shear viscosity of liquid rubidium at three state points (one near the triple point, the other two at expanded states in the liquid regime). They found excellent agreement with

Table V. Comparison of Predicted and Experimental Shear Viscosities for Liquid Rubidium

T, K	ρ, g cm^{-3}	η_{NEMD}, cP	η_{expt},[a] cP
318.9	1.501	0.690	0.644
625.5	1.323	0.215	0.234
939.9	1.181	0.138	0.155

[a] Experimental data from Landolt-Börnstein (Landolt-Börnstein, 1969).

Table VI. NEMD Results for Liquid Sodium

ρ, g cm^{-3}	T, K	γ^*	time steps	η, cP	p, atm	$U^{conf}/(Nk_BT)$
1.006	500	1.00	30 000	0.315	30 552.8	−1.239
		0.64	30 000	0.342	30 391.6	−1.324
		0.36	40 000	0.381	30 267.1	−1.361
		0.16	100 000	0.413	30 196.5	−1.385
		0.09	100 000	0.427	30 174.5	−1.389
1.006	1000	1.00	40 000	0.223	35 924.7	0.0251
		0.64	40 000	0.226	35 871.4	−0.0012
		0.36	100 000	0.221	35 816.4	−0.0077
		0.16	200 000	0.224	35 809.2	−0.0129
		0.09	100 000	0.227	35 811.3	−0.0108
0.954	500	1.00	50 000	0.280	25 959.0	−1.950
		0.64	50 000	0.304	25 790.5	−2.017
		0.36	100 000	0.327	25 705.6	−2.050
		0.16	100 000	0.350	25 653.0	−2.070
		0.09	100 000	0.376	25 632.2	−2.079
0.920	500	1.00	50 000	0.258	23 228.6	−2.392
		0.64	50 000	0.287	23 057.7	−2.460
		0.36	100 000	0.299	22 992.2	−2.488
		0.16	150 000	0.309	22 961.1	−2.504
		0.09	150 000	0.320	22 920.4	−2.517
0.920	1000	1.00	50 000	0.190	28 157.2	−0.595
		0.64	100 000	0.192	28 086.1	−0.611
		0.36	200 000	0.199	28 021.5	−0.622
		0.16	200 000	0.218	27 794.2	−0.665
		0.09	400 000	0.239	27 736.1	−0.676

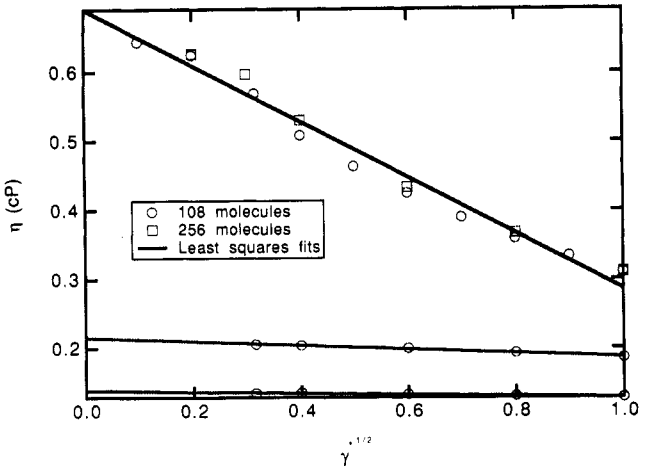

Figure 5. Shear viscosity η of liquid rubidium at the three states given in Table V as a function of the square root of the strain rate γ^*.

experiment (between 7% and 11% deviation) using the Price potential (Price, 1971; Price et al., 1970) for the rubidium intermolecular interaction (see Table V). The strain rate dependent shear viscosities and the least-squares fits to eq 20 are shown in Figure 5.

In another study of liquid metals, Cummings and Morriss (unpublished, reported here for the first time) performed a series of NEMD simulations to determine the shear viscosity of liquid sodium at temperatures of 500 and 1000 K and at densities ranging from 0.9198 to 1.006 g/cm^{-3}. The sodium intermolecular potential used is that of Swanson et al. (Swanson et al., 1982). The simulation results are given in Table VI, where ϵ/k_B = 290 K and σ = 3.56 Å. The shear viscosity is least-squares-fitted to eq

Table VII. Least-Squares Fit of NEMD Results for Liquid Sodium to Theoretical Relationships

ρ, g cm^{-3}	T, K	least-squares fits
1.006	500	$\eta = 0.477 - 0.164\gamma^{*1/2}$ $p = 30176 + 387\gamma^{*3/2}$ $U^{conf}/Nk_BT = -1.395 + 0.153\gamma^{*3/2}$
1.006	1000	$\eta = 0.226 - 0.003\gamma^{*1/2}$ $p = 35801 + 124\gamma^{*3/2}$ $U^{conf}/Nk_BT = -0.0151 + 0.0348\gamma^{*3/2}$
0.954	500	$\eta = 0.408 - 0.130\gamma^{*1/2}$ $p = 25628 + 329\gamma^{*3/2}$ $U^{conf}/Nk_BT = -2.080 + 0.129\gamma^{*3/2}$
0.920	500	$\eta = 0.345 - 0.081\gamma^{*1/2}$ $p = 22924 + 297\gamma^{*3/2}$ $U^{conf}/Nk_BT = -2.517 + 0.121\gamma^{*3/2}$
0.920	1000	$\eta = 0.249 - 0.066\gamma^{*1/2}$ $p = 27814 + 399\gamma^{*3/2}$ $U^{conf}/Nk_BT = -0.662 + 0.077\gamma^{*3/2}$

Table VIII. Newtonian Viscosity, Pressure, and Configurational Internal Energy for Liquid Sodium Obtained from NEMD Simulations and Viscosity from EMD Simulations

state point		NEMD			EMD	η_{expt},
ρ, g cm^{-3}	T, K	p, 10^3 atm	$U^{conf}/(Nk_BT)$	η, cP	η, cP	cP
1.006	500	30.2	−1.395	0.48	0.39	0.50
1.006	1000	35.8	−0.015	0.23	0.24	0.25
0.954	500	25.6	−2.080	0.41	0.36	0.45
0.920	500	22.9	−2.517	0.35	0.33	0.43
0.920	1000	27.8	−0.662	0.25	0.20	0.22

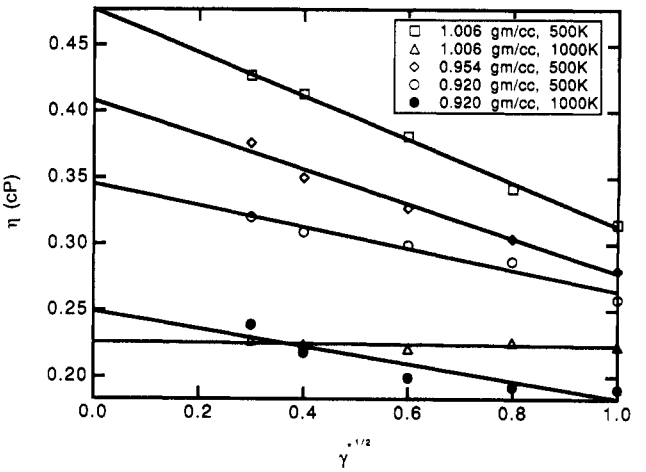

Figure 6. Shear viscosity η of liquid sodium at the five states given in Table VI as a function of the square root of the strain rate γ^*.

20. The pressure p and internal energy u from NEMD simulations are least-squares-fitted to

$$p = p_0 + p_1\gamma^{3/2} \tag{42}$$

$$U^{conf} = U_0 + U_1\gamma^{3/2} \tag{43}$$

where the subscript 0 indicates the zero strain rate limit of each quantity. Equations 42 and 43 are the leading order strain rate dependencies derived theoretically (Kawasaki and Gunton, 1973; Yamada and Kawasaki, 1975; Ernst et al., 1978) and confirmed by extensive simulations (Evans, 1979a, 1981b, 1983a; Evans and Hanley, 1981). The least-squares fits for viscosity, pressure, and configurational internal energy are given in Table VII and the viscosity results are shown in Figure 6.

The lower temperatures are close to the melting transition at each density studied. All the NEMD results for pressure and viscosity are in very good agreement with experiment as shown in Table VIII. EMD GK results were obtained by B. L. Holian of Los Alamos National Laboratory (private communication) on much larger sim-

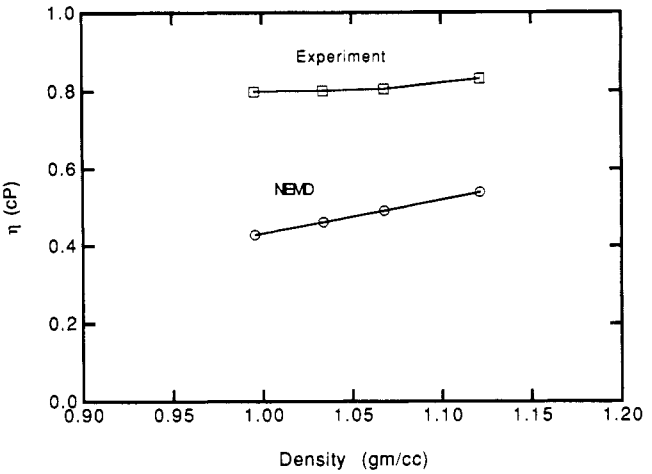

Figure 7. Comparison of the shear viscosity (in cP) of liquid water as a function of density along the 303.15 K isotherm calculated by NEMD (lower points) and experimental values (upper points). The solid lines are drawn as an aid to the eye.

ulation samples. The GK results agree with the NEMD values at the high temperatures but are in disagreement at the low temperatures. This is consistent with the findings of Holian and Evans (Holian and Evans, 1983) that EMD and NEMD simulations exhibit greater agreement the further the state point is from the melting line.

3.1.4. Liquid Water. Cummings and Varner (Cummings and Varner, 1988) performed NEMD simulations of water modeled by the SPC potential (Berendsen et al., 1981) to calculate the shear viscosity of liquid water at 300 K and at densities corresponding experimentally to pressures of 1, 1000, 2000, and 4000 atm. Water exhibits an anomalously small dependence on pressure over the range 1–10 000 atm (often attributed to the strong electrostatic interactions between water molecules), and one of our research goals was to elucidate the microscopic basis for this. Consistent with the only other viscosity calculation for a model water system (a GK EMD calculation by Lie and Clementi (Lie, 1986) for their water potential), the shear viscosities predicted by the SPC potential are about half of the magnitude of the experimental results. However, the slope of the viscosity as a function of pressure (or, equivalently, density) is similar to the experimental data. These results are shown in Figure 7. Surprisingly, suppressing the electrostatic (charge–charge) interactions in the SPC potential (which reduces the potential to a LJ potential and caused the 300 K temperature to correspond to nearly three times the critical temperature) causes little change in the viscosity, suggesting that in the case of liquid water the electrostatic interactions do not contribute significantly to the viscosity.

3.1.5. Supercritical Carbon Dioxide. In a pair of papers, Wang and Cummings (Wang and Cummings, 1989a,b) investigated the shear viscosity, thermal conductivity, and self-diffusion coefficient of supercritical carbon dioxide along the 313 K isotherm using the NEMD algorithms described above. For shear viscosity (Wang and Cummings, 1989a), Wang and Cummings found good agreement with experiment (average error 11%) only with an intermolecular three-site pair potential (Murthy and Singer, 1981) that included both a full representation of the shape of the molecule (one carbon–carbon, four carbon–oxygen, and four oxygen–oxygen site–site interactions) and the electrostatic quadrupolar–quadrupolar interaction. Other potentials considered were a LJ model (Bird et al., 1960) (ignoring both shape and electrostatics) and a potential which modeled carbon dioxide as a homonuclear diatomic (Gibbons and Klein, 1974) (thus including shape but neglecting electrostatics). For densities ranging from 199.8 kg m^{-3} (corresponding to an experimental pressure of 70 bar) to 992.1 kg m^{-3} (500 bar), the three-site potential yielded viscosities with errors (compared to experiment) ranging from 3% to 19%. For thermal conductivity and diffusivity, reasonable agreement with experiment was obtained. The algorithm used for thermal conductivity (Wang and Cummings, 1989b) consisted of eqs 32 and 33 supplemented by the conventional equations for rotational motion, eqs 6. Evans and Murad (Evans and Murad, 1989) recently pointed out that for nonspherical molecules eq 35 neglects a contribution from the rotational motion to the heat current and provided the corrected form of eq 35. We used this corrected form in a recent paper to compute the individual contributions to the thermal conductivity of supercritical carbon dioxide (Wang et al., 1991). For supercritical carbon dioxide, the new contribution identified by Evans and Murad (Evans and Murad, 1989) was found to be small (no more than 20% of the overall thermal conductivity); however, it resulted in better agreement between the NEMD calculation and experimental data.

3.1.6. Alkanes. There has been considerable recent interest in the calculation of the Newtonian transport properties and the non-Newtonian rheology and alkanes. Edberg et al. (Edberg et al., 1987) used NEMD to predict the shear viscosity of *n*-butane and *n*-decane. The alkanes are modeled by inter- and intramolecular potentials which take into account rotations around bonds of rigid length and fixed dihedral angle. Edberg et al. found that the NEMD shear viscosity of liquid *n*-butane at 292 K and 99 bar overestimated the experimental value by 25%, while the NEMD viscosity of liquid *n*-decane at 481 K and essentially 0 bar was within 6% of the experimental result. Maréchal et al. (Maréchal et al., 1987) found a similar result for *n*-butane using a slightly different model and using the EMD GK method. Chynoweth et al. (Chynoweth et al., 1991) performed NEMD sllod simulations on the same model of *n*-butane as Edberg et al. but with 486 molecules rather the 64 molecules used by Edberg et al. They found a much better resolved $\gamma^{1/2}$ behavior in the strain rate dependent shear viscosity and that extrapolating to zero strain rate gave a Newtonian shear viscosity in much better agreement with experiment.

Morriss et al. (Morriss et al., 1991) investigated the non-Newtonian rheology of *n*-decane and *n*-eicosane using the NEMD sllod algorithm and observed shear thickening at elevated strain rates in constant-density simulations. Berker et al. (Berker et al., 1991) performed NEMD sllod simulations of *n*-hexadecane and found that the Newtonian viscosity predicted by their potential model was 1/3 the experimental value. As mentioned in section 2.2 above, Berker et al. also compared the strain rate at which NEMD predicted the onset of shear thinning for *n*-hexadecane and found it agreed with the prediction of Rouse theory for polymer melts.

Rowley and Ely (Rowley and Ely, 1991) used the NEMD sllod algorithm to calculate the Newtonian shear viscosity of *n*-butane and isobutane. The two isomers were modeled as multisite LJ molecules. Experimentally, it is found that the shear viscosity of isobutane increases at a much greater rate with density than *n*-butane. This was also found to be the case in the NEMD simulation, and quantitative agreement with experiment was obtained.

Hoheisel and Würflinger (1991) used the EMD GK method to compute the thermodynamic and transport properties of cyclohexane, which was represented as a

six-center LJ molecule, at saturated liquid and dense high temperature state points. The diffusion coefficient was within 15–30% of experiment and thermal conductivity was within 4–27%. However, the shear viscosity was between 2.7 and 5.4 times lower than experiment, suggesting that the potential model is not very adequate. Corresponding NEMD calculations have not been reported.

3.1.7. Mixtures. There has been only a small effort to date applying NEMD to mixture transport properties. In contrast, the EMD GK methods have been applied to LJ mixtures by several research groups (Jacucci and McDonald, 1975; Schoen and Hoheisel, 1984a,b; Jolly and Bearman, 1980; Hoheisel and Vogelsang, 1988) mostly to calculate self and mutual diffusion coefficients. Heyes and co-workers (Heyes and Preston, 1991a,b; Gardner et al., 1991) have considered LJ mixtures as models for Ar–Kr, Ar–Hg, and Ar–CH_4 mixtures and have calculated mutual and self diffusion coefficients, the thermal conductivity, the cross coefficients (Soret and Dufor effect), and the bulk and shear viscosities. The calculations have been compared with experimental data where available. Typically, good results are predicted for Ar–Kr at both low and high density. For Ar–CH_4 the results at high density are unsatisfactory due to the inadequacy of the simple LJ model for CH_4. This is not surprising in view of the results reported in section 3.1.2.

There have been only three studies to date applying NEMD to mixtures of which the authors are aware. Murad (Murad, 1986) used the isokinetic sllod equations on LJ mixtures to evaluate three sets of mixing rules for mixture viscosities (Kays, van der Waals, and Enskog theory based), finding the simple Kays rule to be quite effective. Wang and Cummings (Wang and Cummings, 1991) performed NEMD sllod simulations to compute the shear viscosity of mixtures of carbon dioxide and ethane at a fixed total density (20 mol/dm^3) and at five compositions ranging from pure carbon dioxide to pure ethane. The carbon dioxide and ethane were modeled as two-center LJ molecules with cross-interaction parameters fitted to the experimental azeotropic data. Wang and Cummings found good agreement with experiment. In particular, the NEMD results showed a plateau in the shear viscosity as a function of composition in agreement with experimental measurements. As already noted in section 2.2, Sarman and Evans (Sarman and Evans, 1991) applied the Evans/Cummings algorithm for thermal diffusion in mixtures finding consistency between NEMD and GK results for Ar–Kr mixtures.

3.1.8. Other Applications of NEMD to Linear Transport Coefficients. We now briefly review other work involving calculation of transport properties using NEMD. Evans and Murad (Evans and Murad, 1989) used NEMD to compute the thermal conductivity of HCl using four models for the pair potential between HCl molecules. The pair potentials included shape, dipole–dipole, dipole–quadrupole, and quadrupole–quadrupole interactions. The NEMD results for saturated liquid HCl at 273 K ranged in error (compared to experiment) from 0% to 22%, depending on the model. Fincham and Heyes (Fincham and Heyes, 1983) used NEMD to compute the shear viscosity of the LJ fluid and used Einstein and GK EMD methods to compute its diffusivity. The results were compared to experimental data on argon and found to be in excellent agreement at high temperatures and densities up to the melting line. Baalss and Hess (Baalss and Hess, 1986) used the NEMD sllod algorithm to study the shear viscosity of a model for nematic liquid crystal (in which all the molecules have their linear axes of symmetry aligned in a common direction called the director). In liquid crystals the shear viscosity in anisotropic since it depends on the angle the director makes with the strain field. Baalss and Hess found good agreement with experimental measurements.

In summary, there has been considerable research performed on applying NEMD algorithms to pure simple fluids and a small effort has been made to apply the algorithms to simple fluid mixtures. There has been a considerable effort in our laboratory and elsewhere to predict transport properties of pure fluids of industrial interest (methane, water, supercritical carbon dioxide, liquid metals, alkanes, and hydrogen chloride). However, efforts to date to use NEMD methods to compute transport properties in mixtures of relevance to the chemical processing industry have been relatively few. We expect to see a much greater emphasis on mixture properties in the near future.

3.2. Rheology of Non-Newtonian Polymeric Fluids. The constitutive relation defining the connection between the stress tensor and the strain field has been the focus of a considerable body of research in polymer rheology, ranging from the predominantly continuum memory function formalism of Astarita and Marrucci (Astarita and Marrucci, 1974) to molecular theories of polymer rheology reviewed by Bird et al. (Bird et al., 1987) and Larson (Larson, 1988). The development of accurate constitutive equations continues to be the focus of many recent publications (for example, Phan-Thien, 1978; Phan-Thien and Tanner, 1977; Papanastasiou et al., 1983; Wedgewood and Bird, 1988). Wedgewood and Bird (Wedgewood and Bird, 1988) point out that constitutive relations fall into one of three categories: empirical formulas, reduced equations for specific flow fields, and equations based on molecular theory derived from statistical mechanical kinetic theories. Each of these parallels a similar technique used in developing equations of state for thermodynamic properties: multiparameter empirical equations of state, corresponding-states methods, and statistical thermodynamic equations of state. Molecular simulation has played a pivotal role in the development of the latter by permitting the direct testing of statistical mechanical theories.

One of the goals of our research is to develop NEMD as an additional tool for use in the development and evaluation of constitutive relations for polymer fluids. This is not a straightforward task given the complexity of the interactions in polymer fluids. We have focused initially on the contribution of internal degrees of freedom to the non-Newtonian rheology of model polymer fluids (Rudisill and Cummings, 1991b). We performed NEMD simulations of rigid and nonrigid dumbbell fluids to compute the contribution of internal degrees of freedom to strain rate dependent shear viscosity and to investigate the transient and steady-state effects on a Couette strain field on model polymer fluids. The model adopted for nonrigid molecules is the finitely extensible nonlinear elastic (FENE) dumbbell commonly used in kinetic theories of polymer solutions (Bird et al., 1987). The FENE dumbbell model consists of two spheres (representing the centers of mass and force for approximately 20 monomer units of a real polymer) connected by a spring force (to model the approximately 20 carbon–carbon bonds between centers of force). The spring force is Hookean at small sphere–sphere separations and diverges to infinity at a finite separation to prevent the dumbbell extending beyond a certain limit. In our work, sphere–sphere intermolecular interactions are modeled as LJ interactions. In Figure 8, we compare the steady-state strain rate dependent shear viscosity of rigid

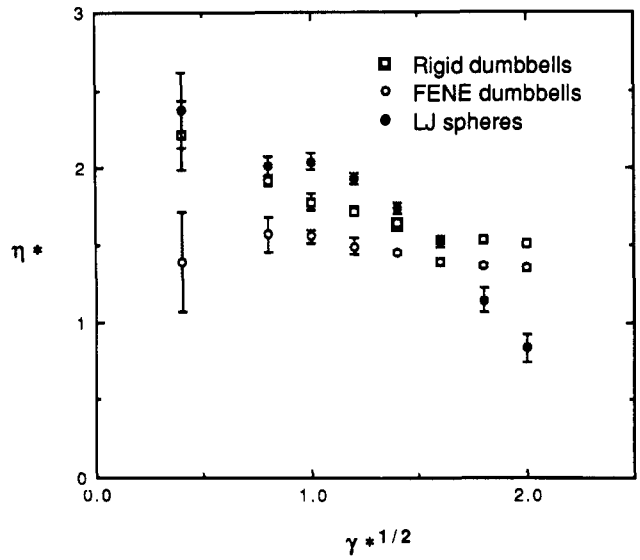

Figure 8. Strain rate dependence of shear viscosity for FENE and rigid dumbbells and spherical molecules. Error bars are omitted where they would be within the symbol.

dumbbells, FENE dumbbells, and a fluid of spheres obtained by severing the bonds in the dumbbells (so that it is a LJ fluid with an atomic density equal to twice the molecular density of the dumbbell fluids). The three fluids are thus in same state with regard to sphere density and are made to be in approximately the same reduced temperature state by using the same T/T_c (where T_c is the critical temperature) for all three systems. The surprising conclusion of the NEMD calculations is that the fluid of LJ spheres exhibits the greatest degree of strain rate dependence, while the most "polymer-like" model, the FENE dumbbell, shows the least strain rate dependence. The transient response of the shear stress shows much the same trend, with the spheres exhibiting the classic non-Newtonian signature of stress overshoot while the FENE dumbbell fluid does not (Rudisill and Cummings, 1991b). Clearly, though, one needs to investigate these phenomena in more realistic models for polymers (such as longer chains) and in polymer solutions where the FENE model is a more accurate rendering of polymeric fluids. Rudisill and Cummings (Rudisill and Cummings, 1991a, 1992) recently extended their work to dilute polymer solutions of FENE dumbbells and chains, finding for the dumbbell models good agreement with kinetic theories for such fluids.

While our work applying NEMD techniques to the study of polymer rheology described above is unique, it should be pointed out that the FENE-type models have been used to investigate polymer rheology in other contexts. Grest and Kremer (Grest and Kremer, 1986; Kremer et al., 1988) used a FENE-based model of polymer solutions to investigate the mean-squared displacement of monomers in polymer chains of length ranging from 10 to 150 spheres. They observed the crossover from small-chain (Rouse) dynamics to long-chain (reptation) dynamics. Bitsanis (Bitzanis and Hadziioannou, 1990) has investigated the conformations and mean-square displacements of polymer melts confined between rigid interfaces using FENE n-mer models (n = 2, 5, 10, 20, 30).

Finally, we note that recently we developed new algorithms for, and performed the first NEMD study of, diffusion in non-Newtonian fluids undergoing shear in a Couette strain field (Cummings et al., 1991). We derived Einstein and GK relations for the diffusion coefficient of a fluid subject to steady-state homeogeneous shear imposed through the use of the sllod algorithm. The derivations hinged on a conjectured solution to the macroscopic convective-diffusion equation for a system under shear. This solution was recently derived by Sarman et al. (Sarman et al., 1991) thus confirming our conjecture. We also conjectured that a simple combination of the sllod and color field algorithms would provide a direct NEMD approach to the calculation of diffusion under shear. Recently, Evans et al. (Evans et al., 1991) showed that this NEMD algorithm is incorrect and derived the correct form. In our study, we investigated a LJ fluid in the non-Newtonian regime and computed the tensor of diffusion coefficients, **D**. We found that this tensor becomes anisotropic in the non-Newtonian regime and that the elements of the tensor of diffusion coefficients show a strong dependence on strain rate, increasing by as much as a factor of 3 over a reduced strain rate of unity. While our study was performed on the LJ fluid in the non-Newtonian regime, experimentally one should expect to observe some of these effects in non-Newtonian polymeric fluids and colloidal suspensions.

Several authors (Evans, 1983b; Heyes, 1986) have pointed out that much of the non-Newtonian rheology of simple fluids discovered by NEMD—such as strain rate dependent shear viscosity, nonzero normal stress differences, viscoelasticity, and shear-induced phase transitions—is qualitatively similar to that usually only associated with polymeric fluids. Heyes (Heyes, 1986) attempted to exploit this similarity by fitting NEMD results on the LJ fluid to empirical rheological constitutive equations.

4. Conclusions

In this paper, we have reviewed the NEMD methods for computing transport properties and described their application to many systems of interest industrially. Future work in our own laboratories will focus on algorithm development for mixtures and applications of these algorithms to supercritical and liquid mixtures of Newtonian fluids. In the area of polymeric materials, our focus will be on polymer solutions (with solvent-mediated interactions modeled through hydrodynamic forces) and on the dependence of rheological properties on chain length. In addition, for comparison with experimental measurements of viscosity for both Newtonian and non-Newtonian fluids, it is convenient to perform the NEMD simulation at isobaric/isokinetic (constant pressure and kinetic energy) ensemble. An isobaric/isokinetic sllod algorithm for planar Couette flow has been developed (Hood et al., 1989) but has thus far been applied only to the SS fluid. Extensions to molecular fluids and chain molecules are presently under study.

Acknowledgment

P.T.C. acknowledges the financial support of the research described in this Review by the National Science Foundation and ICI Films (Industry/University Collaborative Research Grant CBT-8801213) and Comalco Research of Australia. P.T.C. also acknowledges the support of the National Science Foundation through the US/Australia Cooperative Science Program (Grant INT-8913457) for the provision of travel funds to visit the Australian National University where some of the reported research was performed. Computational resources for this research were provided in part by a grant from the National Science Foundation through the Pittsburgh Supercomputing Center (Grant PSCA-880026P). D.J.E. acknowledges the support of a US/Australia Cooperative Research Travel Grant from the Australian Department

of Industry, Technology and Commerce. We are grateful to Professor R. M. Ford for her helpful comments on an earlier version of the manuscript.

Literature Cited

Alder, B. J.; Gass, D. M.; Wainwright, T. E. Studies in Molecular Dynamics. VIII. The Transport Coefficients for a Hard Sphere Fluid. *J. Chem. Phys.* **1970**, *53*, 3813.

Allen, M. P.; Tildesley, D. J. *Computer Simulation of Liquids*; Oxford University Press: Oxford, 1987.

Ashurst, W. T.; Hoover, W. G. Non-Equilibrium Pair Distributions in Simple Fluids. *Bull. Am. Phys. Soc.* **1972**, *17*, 1196.

Astarita, G.; Marrucci, G. *Principles of Non-Newtonian Fluid Mechanics*; McGraw Hill: London, 1974.

Baalss, D.; Hess, S. Nonequilibrium molecular-dynamics studies on the anisotropic viscosity of perfectly aligned nematic liquid crystals. *Phys. Rev. Lett.* **1986**, *57*, 86.

Berendsen, H. J. C.; Postma, J. P. M.; von Gunsteren, W. F.; Hermans, J. Interaction models for water in relation to protein hydration. In *Intermolecular Forces*; Pullman, B., Ed.; Reidel: Dordrecht, 1981; p 331.

Berker, A.; Chynoweth, S.; Klomp, U. C.; Michopoulos, Y. NEMD simulations of the rheological properties of liquid n-hexadecane. *J. Chem. Soc., Faraday Trans.* **1991**. Submitted for publication.

Bird, R. B.; Stewart, W. E.; Lightfoot, E. N. *Transport Phenomena*; Wiley: New York, 1960.

Bird, R. B.; Curtiss, C. F.; Armstrong, R. C.; Hassager, O. *Dynamics of Polymeric Liquids: Kinetic Theory*, 2nd ed.; Wiley: New York, 1987; Vol. 2.

Bitzanis, I.; Hadziioannou, G. Molecular dynamics simulations of the structure and dynamics of confined polymer melts. *J. Chem. Phys.* **1990**, *92*, 3827.

Chialvo, A. A.; Debenedetti, P. G. Use of the McQuarrie equation for the computation of shear viscosity via equilibrium molecular dynamics. *Phys. Rev. A* **1991**, *43*, 4289.

Chialvo, A. A.; Heath, D. L.; Debenedetti, P. G. A molecular dynamics study of the influence of elongation and quadrupole moment upon some thermodynamic and transport properties of linear heteronuclear triatomic fluids. *J. Chem. Phys.* **1989**, *91*, 7818.

Chialvo, A. A.; Cummings, P. T.; Evans, D. J. On the equivalence between McQuarrie and Helfand equations for the determination of shear viscosity from equilibrium molecular dynamics. *Phys. Rev. A.* **1992**. Submitted for publication.

Chynoweth, S.; Klomp, U. C.; Michopoulos, Y. Comment on: Rheology of *n*-alkanes by nonequilibrium molecular dynamics. *J. Chem. Phys.* **1991**, *95*, 3024.

Ciccotti, G.; Jacucci, G.; McDonald, I. R. Transport Properties of Molten Alkali Halides. *Phys. Rev. A* **1976**, *13*, 426.

Ciccotti, G.; Jacucci, G.; McDonald, I. R. "Thought Experiments" by Molecular Dynamics. *J. Stat. Phys.* **1979**, *21*, 1.

Ciccotti, G.; Ferrario, M.; Ryckaert, J. P. Molecular Dynamics of Rigid Systems in Cartesian Coordinates. A General Formulation. *Mol. Phys.* **1982**, *47*, 1253.

Cummings, P. T.; Morriss, G. P. Nonequilibrium Molecular Dynamics Calculation of the Shear Viscosity of Liquid Rubidium. *J. Phys. F: Met. Phys.* **1987**, *17*, 593.

Cummings, P. T.; Morriss, G. P. Shear Viscosity of Liquid Rubidium at the Triple Point. *J. Phys. F: Met. Phys.* **1988**, *18*, 1439.

Cummings, P. T.; Varner, T. L. Nonequilibrium molecular dynamics calculation of the shear viscosity of liquid water. *J. Chem. Phys.* **1988**, *89*, 6391.

Cummings, P. T.; Wang, B. Y.; Evans, D. J.; Fraser, K. J. Non-Equilibrium Molecular Dynamics Calculation of Self Diffusion in a Non-Newtonian Fluid Subject to a Couette Strain Field. *J. Chem. Phys.* **1991**, *94*, 2149.

de Kruif, C. G.; van Lersel, E. M. F.; Vrij, A.; Russel, W. B. Hard Sphere Colloidal Suspensions: Viscosity as a Function of Shear Rate and Volume Fraction. *J. Chem. Phys.* **1985**, *83*, 4717.

Dhont, J. K. G.; van der Werff, J. C.; de Kruif, C. G. The shear thinning behavior of colloidal suspensions. I. Some theoretical considerations. *Physica A* **1989**, *160*, 195.

Edberg, R.; Evans, D. J.; Morriss, G. P. Constrained molecular dynamics simulations of liquid alkanes with a new algorithm. *J. Chem. Phys.* **1986**, *84*, 6933.

Edberg, R.; Morriss, G. P.; Evans, D. J. Rheology of n-alkanes by nonequilibrium molecular dynamics. *J. Chem. Phys.* **1987**, *86*, 4555.

Ernst, M. H.; Cichocki, B.; Dorfman, J. R.; Sharma, J.; van Beijeren, H. Kinetic theory of nonlinear viscous flow in two and three dimensions. *J. Stat. Phys.* **1978**, *18*, 237.

Erpenbeck, J. J. Comparison of Green-Kubo and nonequilibrium calculations of the self-diffusion constant of a Lennard-Jones fluid. *Phys. Rev. A* **1987**, *35*, 218.

Evans, D. J. On the representation of orientation space. *Mol. Phys.* **1977**, *34*, 317.

Evans, D. J. Nonlinear Viscous Flow in the Lennard-Jones Fluid. *Phys. Lett. A* **1979a**, *74*, 229.

Evans, D. J. The frequency dependent shear viscosity of methane. *Mol. Phys.* **1979b**, *37*, 1745.

Evans, D. J. The non-symmetric pressure tensor in polyatomic fluids. *J. Stat. Phys.* **1979c**, *20*, 547.

Evans, D. J. Non-linear viscous flow in two-dimensional systems. *Phys. Rev. A* **1980**, *22*, 290.

Evans, D. J. Non-equilibrium molecular dynamics study of the rheological properties of diatomic liquids. *Mol. Phys.* **1981a**, *42*, 1355.

Evans, D. J. Rheological properties of simple fluids by computer simulation. *Phys. Rev. A* **1981b**, *23*, 1988.

Evans, D. J. Homogeneous NEMD algorithm for thermal conductivity: Application of non-canonical linear response theory. *Phys. Lett. A* **1982**, *91*, 457.

Evans, D. J. Computer 'experiment' for nonlinear thermodynamics of Couette flow. *J. Chem. Phys.* **1983a**, *78*, 3297.

Evans, D. J. Molecular dynamics simulations of the rheological properties of simple fluids. *Physica A* **1983b**, *118*, 51.

Evans, D. J. Nonequilibrium Molecular Dynamics. In *Molecular dynamics simulation of statistical-mechanical systems*; Ciccotti, G., Hoover, W. G., Eds.; Italian Physical Society, North-Holland: Amsterdam, 1986a; pp 221–240.

Evans, D. J. Thermal conductivity of the Lennard-Jones fluid. *Phys. Rev. A* **1986b**, *34*, 1449.

Evans, D. J.; Hanley, H. J. M. Computer simulation of an m-6-8 fluid under shear. *Physica A* **1980**, *103*, 343.

Evans, D. J.; Watts, R. O. Shear-dependent viscosity in simple fluids. *Chem. Phys.* **1980**, *48*, 321.

Evans, D. J.; Hanley, H. J. M. Thermodynamic fluctuation theory for shear flow. *Physica A* **1981**, *108*, 567.

Evans, D. J.; Morriss, G. P. Non-Newtonian molecular dynamics. *Comput. Phys. Rep.* **1984a**, *1*, 297.

Evans, D. J.; Morriss, G. P. Nonlinear response theory for steady planar Couette flow. *Phys. Rev. A* **1984b**, *30*, 1528.

Evans, D. J.; MacGowan, D. M. Addendum to Heat and Matter Transport in Binary Liquid Mixtures. *Phys. Rev. A* **1987**, *36*, 948.

Evans, D. J.; Morriss, G. P. The specific heat of nonequilibrium steady states. *Mol. Phys.* **1987**, *61*, 1151.

Evans, D. J.; Murad, S. Thermal conductivity in molecular liquids. *Mol. Phys.* **1989**, *68*, 1219.

Evans, D. J.; Cummings, P. T. Non-Equilibrium Molecular Dynamics Algorithm for the Calculation of Thermal Diffusion in Simple Fluid Mixtures. *Mol. Phys.* **1990**, *72*, 893.

Evans, D. J.; Morriss, G. P. Numerical test of the Kawasaki distribution function. *Mol. Phys.* **1990a**, *70*, 347.

Evans, D. J.; Morriss, G. P. *Statistical Mechanics of Nonequilibrium Liquids*; Academic Press: New York, 1990b.

Evans, D. J.; Hoover, W. G.; Failor, B. H.; Moran, B.; Ladd, A. J. C. Nonequilibrium molecular dynamics via Gauss's principle of least constraint. *Phys. Rev. A* **1983**, *28*, 1016.

Evans, D. J.; Baranyai, A.; Sarman, S. Response theory for symmetry restricted interactions. *Mol. Phys.* **1991**, in press.

Fincham, D.; Heyes, D. M. Comparisons between experimental argon and Lennard-Jones 12:6 shear viscosities. *Chem. Phys.* **1983**, *78*, 425.

Gardner, P. J.; Heyes, D. M.; Preston, S. R. Molecular dynamics computer simulations of binary Lennard-Jones fluid mixtures: Thermodynamics of mixing and transport coefficients. *Mol. Phys.* **1991**, *73*, 141.

Gibbons, T. G.; Klein, M. L. Thermodynamic properties for a simple model of solid carbon dioxide: Monte Carlo, cell model, and quasiharmonic calculations. *J. Chem. Phys.* **1974**, *60*, 112.

Gillan, M. J.; Dixon, M. The calculation of thermal conductivities by perturbed molecular dynamics simulation. *J. Phys. C: Solid State Phys.* **1983**, *16*, 869.

Gosling, E. M.; McDonald, I. R.; Singer, K. On the Calculation by Molecular Dynamics of the Shear Viscosity of a Simple Fluid. *Mol. Phys.* **1973**, *26*, 1475.

Grest, G. S.; Kremer, K. Molecular dynamics simulation for polymers in the presence of a heat bath. *Phys. Rev. A* **1986**, *33*, 3628.

Gubbins, K. E.; Shing, K. S.; Streett, W. B. Fluid phase equilibria: Experiment, computer simulation and theory. *J. Phys. Chem.* **1983**, *87*, 4573.

Haile, J. M.; Mansoori, G. A., Eds. *Molecular-Based Study of Fluids*; Advances in Chemistry Series 204; American Chemical Society: Washington, DC, 1983.

Heyes, D. M. Non-Newtonian behaviour of simple liquids. *J. Non-Newtonian Fluid Mech.* **1986**, *21*, 137.

Heyes, D. M. Transport coefficients of the Lennard-Jones fluid: Analysis of molecular dynamics data. *Physica A* **1987**, *146*, 341.

Heyes, D. M. Molecular, Brownian and diffusive dynamics: Applications to viscous flows. *Comput. Phys. Rep.* **1988**, *8*, 71.

Heyes, D. M.; Preston, S. R. Equilibrium molecular dynamics computer simulations of the transport coefficients of Ar-CH_4 mixtures. *Mol. Simul.* **1991a**, *7*, 221.

Heyes, D. M.; Preston, S. R. Transport coefficients of Ar-Kr mixtures by molecular dynamics computer simulation. *Phys. Chem. Liq.* **1991b**, *23*, 123.

Hoheisel, C. The shear viscosity of a Lennard-Jones fluid calculated by equilibrium molecular dynamics. *Mol. Phys.* **1985**, *56*, 653.

Hoheisel, C.; Vogelsang, R. Thermal Transport Coefficients for one- and two-component liquids from time correlation functions computed by molecular dynamics. *Comput. Phys. Rep.* **1988**, *8*, 1.

Hoheisel, C.; Würflinger, A. Thermodynamic and transport properties of cyclohexane computed by molecular dynamics with use of a six-center Lennard-Jones potential. *J. Chem. Phys.* **1989**, *91*, 473.

Holian, B. L.; Evans, D. J. Shear viscosities away from the melting line: A comparison of equilibrium and nonequilibrium molecular dynamics. *J. Chem. Phys.* **1983**, *78*, 5147.

Hood, L. M.; Evans, D. J.; Morriss, G. P. Properties of a soft-sphere liquid from non-Newtonian molecular dynamics. *J. Stat. Phys.* **1989**, *57*, 729.

Hoover, W. G.; Ashurst, W. T. Nonequilibrium molecular dynamics. *Theor. Chem. Adv. Perspect.* **1975**, *1*, 1.

Hoover, W. G.; Evans, D. J.; Hickman, R. B.; Ladd, A. J. C.; Ashurst, W. T.; Moran, B. Lennard-Jones Triple-Point Bulk and Shear Viscosities. Green-Kubo Theory, Hamiltonian Mechanics and Nonequilibrium Molecular Dynamics. *Phys. Rev. A* **1980**, *22*, 1690.

Jacucci, G.; McDonald, I. R. Structure and diffusion in mixtures of rare-gas liquids. *Physica A* **1975**, *80*, 607.

Jolly, D. L.; Bearman, R. J. Molecular dynamics simulation of the mutual and self diffusion in Lennard-Jones liquid mixtures. *Mol. Phys.* **1980**, *41*, 137.

Kawasaki, K.; Gunton, J. D. Theory of nonlinear transport processes: Nonlinear shear viscosity and normal stress effects. *Phys. Rev. A* **1973**, *8*, 2048.

Kremer, K.; Grest, G. S.; Carmesin, I. Crossover from Rouse to reptation dynamics: A molecular dynamics simulation. *Phys. Rev. Lett.* **1988**, *61*, 566.

Ladd, A. J. C. Equations of motion for non-equilibrium molecular dynamics simulations of viscous flow in molecular fluids. *Mol. Phys.* **1984**, *53*, 459.

Landolt-Börnstein, H. *Zahlenwerte und Funktionem, 5. Tiel.*; Springer: Berlin, 1969.

Larson, R. G. *Constitutive Equations for Polymer Melts and Solutions*; Butterworth: Boston, 1988.

Lees, A. W.; Edwards, S. F. The Computer Study of Transport Processes Under Extreme Conditions. *J. Phys. C: Solid State* **1972**, *5*, 1921.

Levesque, D.; Verlet, L. Molecular dynamics calculation of transport coefficients. *Mol. Phys.* **1987**, *61*, 143.

Lie, G. C. Consistency check for radical distribution functions of water. *J. Chem. Phys.* **1986**, *85*, 7495.

MacGowan, D. Simulation of diffusion coefficients in binary liquid mixtures. *Mol. Phys.* **1986**, *59*, 1017.

MacGowan, D.; Evans, D. J. Heat and Matter Transport in Binary Liquid Mixtures. *Phys. Rev. A* **1986**, *34*, 2133.

Maitland, G. C.; Rigby, M.; Smith, E. B.; Wakeham, W. *Intermolecular Forces: Their Origin and Determination*; Oxford University Press: Oxford, 1981.

Maréchal, G.; Ryckaert, J.-P.; Bellemans, A. The shear viscosity of n-butane by equilibrium and non-equilibrium molecular dynamics; *Mol. Phys.* **1987**, *61*, 33.

McQuarrie, D. A. *Statistical Mechanics*; Harper and Row: New York, 1976.

Morriss, G. P.; Evans, D. J. Isothermal response theory. *Mol. Phys.* **1985**, *54*, 629.

Morriss, G. P.; Evans, D. J. A constraint algorithm for the computer simulation of complex molecular liquids. *Comput. Phys. Commun.* **1991**, in press.

Morriss, G. P.; Daivis, P. J.; Evans, D. J. The rheology in *n* alkanes: Decane and eicosane. *J. Chem. Phys.* **1991**, *94*, 7420.

Murad, S. The viscosity of dense fluid mixtures: Mixing rules reexamined using nonequilibrium molecular dynamics. *AIChE J.* **1986**, *32*, 513.

Murthy, C. S.; Singer, K. Interaction site models for carbon dioxide. *Mol. Phys.* **1981**, *44*, 135.

Nosé, S. A Molecular Dynamics Method for Simulations in the Canonical Ensemble. *Mol. Phys.* **1984a**, *52*, 255.

Nosé, S. A Unified Formulation of the Constant Temperature Molecular Dynamics Methods. *J. Chem. Phys.* **1984b**, *81*, 511.

Papanastasiou, A. C.; Scriven, L. E.; Macosko, C. W. An integral constitutive equation for mixed flows: viscoelastic characterization. *J. Rheol.* **1983**, *27*, 387.

Phan-Thien, N. A nonlinear network viscoelastic model. *J. Rheol.* **1978**, *22*, 259.

Phan-Thien, N.; Tanner, R. I. A new constitutive equation derived from network theory. *J. Non-Newtonian Fluid Mech.* **1977**, *2*, 353.

Prausnitz, J. M.; Lichtenthaler, R. N.; de Azevedo, E. G. *Molecular Thermodynamics of Fluid Phase Equilibria*, 2nd ed.; Prentice-Hall: Englewood Cliffs, NJ, 1986.

Price, D. L. Effects of a volume-dependent potential on equilibrium properties of liquid sodium. *Phys. Rev. A* **1971**, *4*, 358.

Price, D. L.; Singwi, K. S.; Tosi, M. P. Lattice dynamics of alkali metals in the self-consistent screening theory. *Phys. Rev. B* **1970**, *2*, 2983.

Rowley, R. L.; Ely, J. F. Non-equilibrium molecular dynamics simulations of structured molecules. *Mol. Phys.* **1991**, *72*, 831.

Rudisill, J. W.; Cummings, P. T. Brownian dynamics simulation of model polymer fluids in shear flow II. Bead-spring chain models. *J. Non-Newtonian Fluid Mech.* **1991a**. Submitted for publication.

Rudisill, J. W.; Cummings, P. T. The contribution of internal degrees of freedom to the non-Newtonian rheology of model polymer fluids. *Rheol. Acta* **1991b**, *30*, 33.

Rudisill, J. W.; Cummings, P. T. Brownian dynamics simulation of model polymer fluids in shear flow I. Dumbbell models. *J. Non-Newtonian Fluid Mech.* **1992**, *41*, 275.

Ryckaert, J. P.; Bellemans, A. Molecular dynamics of liquid alkanes. *Discuss. Faraday Soc.* **1978**, *66*, 95.

Ryckaert, J. P.; Ciccotti, G.; Berendsen, H. J. C. Numerical Integration of the Cartesian Equations of Motion of a System with Constraints: Molecular Dynamics of *n*-alkanes. *J. Comput. Phys.* **1977**, *23*, 327.

Sarman, S.; Evans, D. J. Thermal Diffusion in Argon/Krypton Mixtures. *Phys. Rev. A* **1991**. Submitted for publication.

Sarman, S.; Evans, D. J.; Cummings, P. T. Comment on: Nonequilibrium molecular dynamics calculation of self-diffusion in a non-Newtonian fluid subject to a Couette strain field. *J. Chem. Phys.* **1991**, *95*, 8675.

Schoen, M.; Hoheisel, C. The mutual diffusion coefficient D_{12} in binary liquid model mixtures. Molecular dynamics calculations based on Lennard-Jones potentials. I. The method of determination. *Mol. Phys.* **1984a**, *52*, 33.

Schoen, M.; Hoheisel, C. The mutual diffusion coefficient D_{12} in binary liquid model mixtures. A molecular dynamics study based on Lennard-Jones potentials. II. Lorentz-Berthelot. *Mol. Phys.* **1984b**, *52*, 1042.

Simmons, A. D.; Cummings, P. T. Non-Equilibrium Molecular Dynamics Simulation of Dense Fluid Methane. *Chem. Phys. Lett.* **1986**, *129*, 92.

Singer, K.; Singer, J. V. L.; Fincham, D. Determination of the Shear Viscosity of Atomic Liquids by Non-Equilibrium Molecular Dynamics. *Mol. Phys.* **1980**, *40*, 515.

Swanson, R. E.; Straub, G. K.; Holian, B. L.; Wallace, D. C. Thermodynamic properties of solid sodium from quasiharmonic lattice dynamics and molecular dynamics. *Phys. Rev. B* **1982**, *25*, 7807.

van der Werff, J. C.; de Kruif, C. G.; Dhont, J. K. G. The shear thinning behavior of colloidal suspensions. II. Experiments. *Physica A* **1989**, *160*, 205.

Wang, B. Y.; Cummings, P. T. Non-equilibrium Molecular Dynamics Calculation of the Shear Viscosity of Carbon Dioxide. *Int. J. Thermophys.* **1989a**, *10*, 929.

Wang, B. Y.; Cummings, P. T. Non-Equilibrium Molecular Dynamics Calculation of the Transport Properties of Carbon Dioxide. *Fluid Phase Equilib.* **1989b**, *53*, 191.

Wang, B. Y.; Cummings, P. T. Non-equilibrium molecular dynamics calculation of the shear viscosity of carbon dioxide/ethane mixtures. *Chem. Eng. Sci.* **1991**. Submitted for publication.
Wang, B. Y.; Cummings, P. T.; Evans. D. J. Non-Equilibrium Molecular Dynamics Study of Molecular Contributions to the Thermal Conductivity of Carbon Dioxide. *Mol. Phys.* **1991**, in press.
Wedgewood, L. E.; Bird, R. B. From molecular models to the solution of flow problems. *Ind. Eng. Chem. Res.* **1988**, *27*, 1313.
Williams, D. E. Nonbonded potential parameters derived from crystalline aromatic hydrocarbons. *J. Chem. Phys.* **1967**, *47*, 4680.
Yamada, T.; Kawasaki, K. Application of mode-coupling theory to nonlinear stress tensor in fluids. *Prog. Theor. Phys.* **1975**, *53*, 111.
Zwanzig, R. Time Correlation Functions and Transport Coefficients in Statistical Mechanics. *Annu. Rev. Phys. Chem.* **1965**, *16*, 67.

Received for review June 12, 1991
Revised manuscript received January 13, 1992
Accepted February 1, 1992

KINETICS AND CATALYSIS

De-SO_x Catalyst: The Role of Iron in Iron Mixed Solid Solution Spinels, $MgO{\cdot}MgAl_{2-x}Fe_xO_4$

Jin S. Yoo,* Alak A. Bhattacharyya, and Cecelia A. Radlowski
Amoco Research Center, Amoco Chemical Company, P.O. Box 3011, Naperville, Illinois 60566

John A. Karch
UOP, 25 E. Algonquin Road, Des Plaines, Illinois 60017-5017

The iron mixed solid solution spinels, $MgO{\cdot}MgAl_{2-x}Fe_xO_4$, were prepared by the coprecipitation method, and the role of iron in these spinels was examined for the de-SO_x chemistry. The iron in the mixed spinels exhibited a dual function, namely, the catalytic oxidation of SO_2 to SO_3 and the dramatic lowering of the sulfate reduction temperature. In short, the iron mixed solid solution spinels performed much better as a de-SO_x catalyst than their single solid solution counterpart without iron, $Ce/MgO{\cdot}MgAl_2O_4$. The fractional substitution of the Al atom in the spinel structure ($x \leq 0.4$) resulted in overcoming a drawback of sulfur accumulation inherent in the solid solution spinel. Sulfur tends to build up rather quickly in the de-SO_x cycle test with the solid solution spinel catalyst without iron. The iron mixed solid solution spinels impregnated with cerium, $Ce/MgO{\cdot}MgAl_{2-x}Fe_xO_4$, displayed an even better de-SO_x function and an excellent steam stability as well.

Introduction

Recently, the sulfate of the stoichiometric spinel, $MgAl_2O_4$, was studied using IR spectroscopy and vacuum microbalance techniques, and it was shown that the spinel is the best sulfur-transfer catalyst for reducing SO_x emission (Waqif et al., 1991a,b). There have been other reports concerning the spinel phase structure (Kwestroo et al., 1959), the solid-state properties (Narasimhan and Swamy, 1980), and the catalytic activities (Narasimhan and Swamy, 1982, 1976) of the iron mixed stoichiometric spinel, $MgAl_{2-x}Fe_xO_4$, along with the acid–base properties of aluminum–magnesia mixed oxides (Lercher et al., 1984).

Much of the literature revolves around the fractional replacement of aluminum in the spinel structure by iron. The mixed stoichiometric spinel, $MgAl_{2-x}Fe_xO_4$, varies in an interesting manner as a function of x and forms the solid solution in two concentration ranges of x: $0 \leq x \leq 0.4$ and $1.3 \leq x \leq 2.0$ (Narasimhan and Swamy, 1980). The iron mixed stoichiometric spinels, $MgAl_{2-x}Fe_xO_4$, as well as the iron mixed solid solution spinels, $MgO{\cdot}MgAl_{2-x}Fe_xO_4$, were prepared and evaluated for the following key reactions involved in the de-SO_x process (Yoo et al., 1991, 1990a–c, 1988). This work is particularly focused on the sulfate reduction reaction, which is believed to be the rate-determining step in the de-SO_x cycle.

$$SO_2 + O_2 \rightleftarrows SO_3 \quad (1)$$

$$SO_3 + MgO \rightarrow MgSO_4 \quad (2)$$

$$MgSO_4 + H_2 \rightarrow MgO + H_2S + H_2O \quad (3)$$

The single solid solution spinel with cerium, $Ce/MgO{\cdot}MgAl_2O_4$, tends to accumulate sulfur for each cycle due to insufficient sulfur removal in the sulfate reduction half cycle (Bhattacharyya et al., 1988). However, the iron mixed solid solution spinels were able to overcome this drawback and exhibited an excellent catalyst rejuvenation by significantly lowering the temperature required for the sulfate reduction. These observations prompted us to explore the effectiveness of these iron mixed solid solution spinels as a de-SO_x catalyst.

Experimental Section

The spinel materials studied in this work can be classified into the following four types: stoichiometric spinel, $MgAl_2O_4$; iron mixed stoichiometric spinel, $MgAl_{2-x}Fe_xO_4$; single solid solution spinel, $MgO{\cdot}MgAl_2O_4$; iron mixed solid solution spinel, $MgO{\cdot}MgAl_{2-x}Fe_xO_4$.

The mixed stoichiometric spinels and the mixed solution spinels in which Al atom was fractionally substituted by iron were prepared according to the coprecipitation method described for $MgAl_{0.6}Fe_{1.4}O_4$ below.

A magnesium nitrate solution was prepared by dissolving 512.8 g (2.0 mol) of $Mg(NO_3)_2{\cdot}6H_2O$ in about 100 mL of

*To whom correspondence should be addressed.

0888-5885/92/2631-1252$03.00/0